

PRELIMINARY DESIGN OF THE MAGNETIC SYSTEM FOR  
ORBIT CORRECTION IN LEP

Ph. Lebrun

1. INTRODUCTION
2. BASIC REQUIREMENTS
3. THE CHOICE OF MAGNET GEOMETRY
4. THE CHOICE OF CURRENT DENSITIES
5. PROPOSED MAGNET DESIGNS

APPENDIX 1

APPENDIX 2

APPENDIX 3

APPENDIX 4

REFERENCES

TABLES

FIGURES

## 1. INTRODUCTION

It may seem premature to design hardware components for LEP at a time when some basic parameters of the machine are not yet finalized. However, general methods and design principles remain valid throughout changes in machine parameters, and are therefore worth being presented as such. This is the spirit of this work.

After putting together a consistent set of requirements for the orbit correction magnetic system, on the basis of presently available data, the choice of a magnet geometry fulfilling these requirements is discussed. A method for technico-economical optimization of the system is then presented, leading to the choice of current densities. Finally, preliminary designs for the orbit correction magnets are given with emphasis on the specific points requiring further study and the possibility of exploring alternate technical options.

## 2. BASIC REQUIREMENTS

The principle of closed orbit correction in LEP version 11<sup>1)</sup> has been described in a note<sup>2)</sup> which constitutes the basis for our work. The technological framework used to set design boundaries is essentially that of the Pink Book<sup>3)</sup>, and the relevant additions or modifications to it at this date.

Function permits classifying corrector magnets in two classes: correctors for horizontal orbit called CH (i.e. vertical field magnets), and correctors for vertical orbit called CV (i.e. horizontal field magnets). Corrector magnets are also of three different types according to their position in the machine: standard lattice correctors, RF-section correctors, and interaction region correctors. This yields six classes of requirements for the orbit correction magnets given in table 1 with the number of units in each class. As far as standard lattice CH magnets are concerned, the alternative solution of backleg windings on the main dipole magnets has been rejected, mainly because of large hysteresis<sup>23)</sup>. A common design requirement for all magnets is their magnetic length of 0.5 m, allowing their maximum field levels to be calculated from the requirements of field integral given in reference 2). The gap of each magnet must accommodate the LEP vacuum chamber, equipped with its lead shielding and bakeout insulation; vacuum chamber design is not finalized at present but the following guidelines<sup>4)</sup> have been used:

- i) in the standard lattice correctors, the vacuum chamber has the same quasi-elliptical cross-section as in the lattice quadrupoles; the overall magnet aperture dimensions are 200 mm horizontally and 100 mm vertically, including fabrication and alignment tolerances<sup>5)</sup>.
- ii) in the straight RF-sections, one intends to use standard vacuum chamber as much as possible; only between the installed RF cavities will one use round 100 mm I.D. chamber, requiring a circular aperture about 120 mm in diameter. Since the sections to be equipped with circular and elliptical chambers are not yet defined, and may

change as RF cavities are installed gradually in the machine, the RF-section corrector magnets must be tailored to the biggest aperture requirements, namely 200 mm horizontally and 120 mm vertically.

- iii) close to interaction regions, the vacuum chamber design is even less defined; it will be fixed only at a later date. At present, a round chamber of 160 mm I.D. is envisaged as one possibility, requiring a circular aperture 180 mm in diameter. This value was taken as the basis for preliminary design work.
- iv) in all cases the longitudinal positions of the corrector magnets in the machine are such that vacuum chamber singularities (compensator bellows, connection flanges, pumping ports, cooling water in- and outlets, electrical feedthroughs) fall outside the magnet apertures.

The maximum field inhomogeneity  $\Delta B/B_{\max}$  tolerable in each corrector magnet is 5% in the useful region of the aperture<sup>2)</sup>, appearing in table 1. In all cases the setting accuracy and stability has to be better than 1% of the maximum field value, and the maximum ramping rate expected is 1% per second.

Each magnet will be energized by its own dedicated power supply, through cables running along the tunnel. The power supplies serving two adjacent half-octants will be located in a surface service building at interaction points 1,2,6,7,8; for interaction points 3,4,5 which will have no access pit to the surface, the power supplies will be installed in a cave at the level of the machine tunnel<sup>6)</sup>. The length of cabling involved can be estimated from table 2, which gives the approximate longitudinal positions of the correction magnets in one octant, as obtained from the AGS structure of LEP version 11<sup>1)</sup>; the LEP layout imposes long cables and thus favours low design currents.

### 3. THE CHOICE OF MAGNET GEOMETRY

The overall length of the orbit correction magnets, defined by the longitudinal space available in the machine, is a fixed boundary to the designer; optimal design then consists in finding a two-dimensional distribution of excitation coils and magnetic yoke which gives the wanted field level and quality, while keeping to a minimum the transverse dimensions and hence the mass (and cost) of the magnets. Other important parameters in selecting a geometry are magnet end effects, non linear effects at low excitation (remanent field, variation of permeability), stray field, transient effects upon ramping, mechanical structure stability, manufacture and assembly characteristics of coils and yoke.

In the following, three magnet geometries able to generate homogeneous dipole fields are investigated (fig. 1):

- i) a conventional 'pole-and-return-yoke' geometry, similar to that of the radial field magnets in the ISR,
- ii) a so-called 'window-frame' geometry,
- iii) a 'horse-shoe' geometry.

In order to compare the respective merits of each solution, a common set of design requirements was established:

- gap = 200 mm (corresponding to a lattice CV corrector)
- field strength = 0.05 T
- field homogeneity better than 5% over rectangular aperture of ( $\pm 55$  mm) x ( $\pm 30$  mm)
- copper coils with average current density =  $2 \text{ A mm}^{-2}$
- yoke made of unalloyed low-carbon steel, identical to that used for ISR magnets.

In each case, the two-dimensional magnetic field in the transverse plane was calculated by program POISSON<sup>7)</sup>. Starting from simple configurations fitting tightly around the vacuum chamber, two-dimensional magnet designs were progressively refined in order to achieve the desired field quality.

For the 'conventional' geometry (fig. 2), field calculations show that with optimized shims, a minimum pole width of 240 mm is necessary to fulfil the requirements on field quality. The flux return yoke, which increases the transverse dimensions of the magnet, suppresses all stray field in the transverse plane. The excitation coils are simple in design and construction.

The 'window-frame' geometry (fig. 3) yields excellent two-dimensional field quality with a simple yoke design. In practice, there are two ways of building excitation coils for such a yoke geometry: bedstead or racetrack. The latter, although simpler to manufacture and assemble, requires more copper and hence increases capital and operation costs of the magnets. Moreover, the current return path in the racetrack coils produces stray field around the magnet itself. However, the two-dimensional field quality in the useful region is the same for both options.

The 'horse-shoe' geometry (fig. 4) permits suppressing one of the two racetrack coils of the 'window-frame' magnet. Yoke and coil designs are rather straightforward; a simple shim is sufficient to obtain the desired field homogeneity in the gap.

The results of this comparative study are summarized in table 3: the 'conventional' and 'window-frame' geometries are comparable as regards mass of copper and power consumption, while the 'horse-shoe' geometry allows a gain of about a factor of 2 on both parameters. Therefore, it appears that the latter solution, which leads to a more economical design, is to be preferred. However, before a final choice is made, other aspects have to be investigated.

#### Stray field

The simple racetrack coils of the 'horse-shoe' and 'window-frame' geometries produce stray field around the magnet. A calculation by POISSON yields a map of the flux lines in the transverse plane (fig. 5), showing the decay of the field strength with increasing distance from the centre of the magnet. Ways of reducing this stray field by magnetic shielding have been investigated, with little success; significant improvements can only be achieved by using iron shields comparable in size to the magnet yoke, which is both uneconomic and impractical.

Therefore, such a stray field seems unavoidable; however, it should not bring important adverse effects (magnetic forces, field perturbations), since its strength,  $2 \times 10^{-3}$  T at 1 m from the magnet centre, is comparable to the stray fields of adjacent magnets.

#### Non linear effects at low excitation

The magnets studied here, being correction elements, are expected to operate mostly at low excitation, say 10% of their nominal levels. Hence it is essential to study the degradation of field quality in those conditions, due to variation of magnetic permeability and remanent field in the iron: the former effect can be taken into account by POISSON, but not the latter. The results of POISSON calculations performed on the same 'horse-shoe' geometry (i) at 100% excitation using the upper branch of the steel permeability curve (fig. 6) and (ii) at 10% excitation using the lower branch of the permeability curve, appear in fig. 7: the gradient produced by the difference in the flux path lengths in the low permeability regions degrades the field homogeneity, however still within acceptable limits. Moreover, the coercive force in the steel tends to compensate for this effect<sup>8)</sup>.

More critical than the field gradient inhomogeneity is the error in the central field resulting from remanent effects:

$$B_{rem} = \frac{\mu_0}{2} \int_{steel} H_c \, dl$$

where the coercive force  $H_c$  depends on the maximum magnetization previously undergone by the steel. Assuming that the magnet has been previously excited to its maximum level, one can then calculate  $B_{rem}$  from POISSON field maps and the measured values of coercive force versus initial magnetization of the steel (fig. 8)<sup>8)</sup>. For a yoke thickness of 20 mm, the central remanent field is calculated to be about  $10^{-4}$  T, i.e. 2% of the maximum field. The absolute value of the remanent field can be further reduced, if required, by:

- i) increasing the yoke thickness, thus lowering  $H_c$ ;
- ii) use of silicon-steel instead of unalloyed low-carbon steel for the yoke (Appendix 1).

The presence of the remanent field will lead to a hysteresis effect, depending on the excitation history of each magnet, which will affect the reproducibility of the orbit correction. This problem could be solved, as for the ISR, by the introduction of a numerical model describing the phenomenon.

#### Mechanical construction

The dimensions of the yoke being defined by magnetic requirements, it remains to check its mechanical stability upon magnetic forces. A typical requirement is that the relative gap closure at maximum excitation should be small as compared to the tolerance on field inhomogeneity. Due to the relatively low field level in the magnet, the magnetic forces produce a maximum gap closure of only a few  $\mu\text{m}$ , which has a negligible influence on the field quality.

The simple geometry and small thickness of the pole pieces, as well as the slow ramping rates to be encountered, suggest a massive steel plate construction, rather than the usual stacked lamination solution, in which the punching of sheets would result in a considerable loss of material (typically twice the amount of material in the yoke) and a more expensive construction. Moreover, a yoke made of three bolted plates would permit easy assembly of the coil around the yoke backleg. An estimate of the field error due to eddy currents induced in massive pole pieces upon ramping the magnets (Appendix 2) shows that, in principle, the solid-cored solution is feasible.

The available standards<sup>9,10)</sup> on form and dimension tolerances of rolled metallurgical products seem to show that thickness and planeity of 20 mm sheet are precise enough to use it as rolled for construction of the pole pieces. However, should these tolerances not be met, one-pass milling of the plate surface has proved to be a simple, inexpensive and satisfactory issue<sup>11)</sup>.

The mechanical tolerances on coil fabrication and position have also been investigated: the field error created by a gap of 2 mm between coil and yoke (i.e. 1 mm surface insulation + 1 mm tolerance) can be easily compensated by machining a small shoulder in the pole piece (fig. 10).

On the whole, it appears that among the different options studied the 'horse-shoe' geometry fulfils all technical requirements for orbit correction magnets in the most simple and economical way.

#### 4. THE CHOICE OF CURRENT DENSITIES

The magnetic system for orbit correction in LEP includes the magnets proper, their cables and power supplies; the aim is to minimize the total (i.e. capital plus operation) cost of the system, according to the same basic rules as applied to other LEP components<sup>12)</sup>:

- i) the costs are expressed in constant currency units; the effects of inflation and actualization are neglected.
- ii) operation costs are calculated on the basis of 30'000 hours (i.e. 3'000 hours per year during 10 years) at a beam energy of 85 GeV.
- iii) the cost of electrical power is assumed to be 70 SF per MWh.
- iv) cooling and ventilation costs in the LEP tunnel amount to about 1'000 SF per kW of power extracted; for distributed loads, as well as lumped loads of moderate power, air and water cooling costs are comparable; due to the good heat exchange between air and cooling water in the tunnel, all the heat added to the air will transfer and ultimately be extracted in the cooling water<sup>13)</sup>.

The following remarks apply:

- i) the magnets considered being correction elements, their r.m.s. excitation level over operating lifetime will be only a fraction of the maximum, of the order of 20%<sup>14)</sup>; the corresponding average electrical power consumption is then only 4% of the rated power, yielding low integrated operating costs which can be neglected as compared to capital costs.

- ii) in the range considered, and provided one accepts the present safe limit of 120 V maximum output voltage<sup>15)</sup>, it appears that the cost of power supplies shows little dependence to output current or output power<sup>16)</sup>. This can be accounted for by the relative importance of the control circuitry with respect to the power stage of the supplies. It is then legitimate to exclude the cost of the power supplies from the cost function to be minimized.
- iii) remaining contributions to the cost function are thus magnet (yoke and coil) and cable (material and installation) costs. The yoke, being essentially determined by magnetic requirements, has no significant influence on the optimum. As for the cables, installation costs are not expected to be strongly dependent on their type and cross-section, in the range of low currents (a few A) and hence small cross-sections (a few mm<sup>2</sup>) considered. The cost function then consists only of the cost of copper in the coils and in the cables.
- iv) a survey of small cross-section biconductor cables meeting CERN standard requirements (see Appendix 3) shows that the equivalent cost of copper in such cables is in the range of 30 to 35 SF/kg, i.e. about the same as the cost of copper in an epoxy-impregnated magnet coil of simple geometry<sup>17)</sup>. Therefore, minimizing the total cost reduces to minimizing the total mass of copper m in the cable+coil system.

Which set of operating current I and current densities  $j_M$  in the magnet and  $j_C$  in the cable will minimize  $m = m_M + m_C$  under the condition  $U = U_M + U_C \leq 120$  V?

By definition

$$I = j_M S_M = j_C S_C \quad (I)$$

with  $S_M$  = conductor cross-section in magnet  
 $S_C$  = conductor cross-section in cable

$$m_M = \frac{\mu \wedge N I}{\sigma_M} \quad (II)$$

with  $\mu$  = mass density of conductor  
 $\wedge$  = length of one turn in the magnet  
 $(NI)$  = number of ampère-turns

$$m_C = \frac{\mu l_C^* I}{j_C} \quad (III)$$

with  $l_C^*$  = average length of cable per magnet.

$$\frac{I}{j_M} = \frac{R_M}{j_M} = \frac{\rho \wedge N I}{U - U_C} = \frac{\rho \wedge N I}{U - \rho j_C l_C^*} \quad (IV)$$

with  $\rho$  = resistivity of conductor  
 $l_C$  = maximum length of cable per magnet.

From equations (III) and (IV):

$$m_c = \frac{\mu l_c^*}{j_c} \frac{\rho \Lambda N I j_M}{U - \rho l_c j_c}$$

so that

$$m = m_M + m_c = \mu \Lambda N I \left[ \frac{1}{j_M} + \frac{\rho l_c^* j_M}{j_c (U - \rho l_c j_c)} \right]$$

depends only on the variables  $j_M$  and  $j_c$ .

The minimum of  $m$  is found by writing that:

$$\left. \begin{aligned} \frac{\partial m}{\partial j_M} \Big|_{j_c} &= 0 \\ \frac{\partial m}{\partial j_c} \Big|_{j_M} &= 0 \end{aligned} \right\} \text{simultaneously}$$

This yields

$$\begin{cases} j_M^{\text{opt}} = \frac{U}{2 \rho \sqrt{l_c l_c^*}} \\ j_c^{\text{opt}} = \frac{U}{2 \rho l_c} \end{cases}$$

from which one can calculate the optimal current:

$$I^{\text{opt}} = \frac{\Lambda N I}{\sqrt{l_c l_c^*}}$$

and hence the conductor cross-sections  $S_M^{\text{opt}}$  and  $S_C^{\text{opt}}$ . The number of turns in the winding is then:

$$N^{\text{opt}} = \frac{\sqrt{l_c l_c^*}}{\Lambda}$$

and

$$m_M^{\text{opt}} = m_C^{\text{opt}} = \frac{2 \mu \rho \Lambda N I}{U} \sqrt{l_c l_c^*}$$

This relation clearly demonstrates that the maximum output voltage of the power supply affects the total mass of copper, and hence the economics of the system; this is discussed in more detail in Appendix 4.

It is worth noting that in optimized conditions half of the total available voltage drop occurs in the magnet winding, and the other half in the longest cable.

The average and maximum lengths of cable feeding CV and CH magnets can be estimated from table 2 and ref. 6); the corresponding optimal values for current densities, operating current and conductor cross-sections appear in table 4.

For the lattice corrector magnets, the maximum output voltage of the power supply imposes moderate current densities in both coils and cables. However, due to the shorter length of the RF-section magnet cables, this condition is not restrictive enough to define realistic values of current densities in the windings of these magnets. Other technological considerations need then to be considered, namely the power dissipation and resulting temperature rise in the coils.

#### Temperature gradient across coil

Consider a coil of rectangular cross-section, of width  $x$  equal to the gap of the magnet, and thickness  $e$ . Let  $q$  be the power dissipation per unit volume, and  $\tilde{K}$  the equivalent thermal conductivity in the coil. The steady-state temperature difference between the centre and the surface of the coil is then<sup>18)</sup>:

$$\Delta T_1 = \frac{q e^2}{8 \tilde{K}}$$

Since  $q = \rho j_M^2 f$  and  $e = \frac{N S M}{f x}$   
with  $f$  = conductor filling factor in coil,

then

$$\Delta T_1 = \frac{f}{8 \tilde{K} \rho} \left( \frac{N I}{x} \right)^2$$

For a given magnet,  $\Delta T_1$  depends only on the filling factor  $f$  and equivalent thermal conductivity  $\tilde{K}$ ; it is independent of the current density  $j_M$  in the coil.

The filling factor  $f$  which can be reasonably achieved in epoxy-impregnated coils wound from enamelled (grade 2) round copper wire appears in fig. 11 as a function of the wire cross-section<sup>19)</sup>. Fig. 12 shows the ratio of the equivalent thermal conductivity of the coil  $\tilde{K}$  to the thermal conductivity of the insulation  $K_i$  as a function of the filling factor  $f$ , for round wire windings<sup>18)</sup>.

From this data, one can plot the equivalent thermal conductivity ratio  $\tilde{K}/K_i$  of the coil versus the cross-section of the wire (fig. 13): using a bigger wire increases both the filling factor and the equivalent thermal conductivity ratio and hence decreases the temperature difference  $\Delta T_1$  (fig. 14). For all the magnets considered, the values of  $\Delta T_1$  obtained with wire cross-sections above  $1 \text{ mm}^2$  are acceptable ( $\Delta T_1 < 15 \text{ K}$ ).

#### Air or water cooling at the surface of the windings?

In the case of water cooling, the temperature at the surface of the windings will be very close to that of the coolant, which can be kept sufficiently low, thanks to the good heat transfer coefficient and high specific heat of water. Therefore, water cooling at the surface of the windings is not expected to set tight constraints on power dissipation and hence current densities in the coils.

However, air cooling is worth being considered for it could bring several technical simplifications to coil design: besides the suppression of water piping and connections, a coil cooled by natural convection in still air is intrinsically safe against overheating, and hence does not require temperature interlocks and the associated cabling.

Let  $h$  be the heat transfer coefficient between coil surface and air; the steady-state temperature drop occurring at the surface is

$$\Delta T_2 = \frac{P_M}{h \Sigma}$$

with  $P_M$  = steady-state power dissipation in the coil

$\Sigma$  = heat exchange surface area.

For the coil geometry considered, one can take:

$$\Sigma \approx 2 \Lambda x$$

and thus:

$$\Delta T_2 \approx \frac{\rho N I}{2 h x} j_M$$

so that, for a given magnet,  $\Delta T_2$  depends only on  $h$  and  $j_M$ .

During machine operation, the velocity of air in the LEP tunnel will be about  $1 \text{ m s}^{-1}$ , yielding a heat transfer coefficient of about  $9 \text{ W m}^{-2} \text{ K}^{-1}$  (20). However, to cope with all situations, the more conservative value of  $6 \text{ W m}^{-2} \text{ K}^{-1}$  used for natural convection in still air<sup>18)</sup> will be used in the calculations. Fig. 15 shows calculated values of  $\Delta T_2$  for orbit correction magnets as a function of the current density in the coils: acceptable values of  $\Delta T_2$  (i.e. below 40 K) can only be achieved with very low current densities, at the expense of a large amount of copper in the coils. This situation could be improved by increasing either  $\Sigma$  (finned radiator plate) or  $h$  (forced-flow cooling, heat pipe); both solutions require further investigation. In the following we shall keep to the use of a water-cooled radiator around the coils.

#### Maximum power dissipation

Practical limits can be set on the current densities in the windings by the power drawn from the supply at maximum excitation:

$$P_M = \rho \Lambda (NI) j_M$$

This relation is shown graphically on fig. 16 for the different types of orbit correction magnets. The technology presently envisaged for the power supplies tends to limit their maximum output power to about  $1 \text{ kW}$ <sup>22)</sup>, which we shall take as upper design limit. For the RF-section magnets, a rated power of 500 W (excluding the power dissipation in the cable) is obtained with a current density of about  $3 \text{ A mm}^{-2}$  in the windings. For the interaction region magnets, which need more ampère-turns and are located closer to their power supplies, a rated power of 700 W corresponds to about  $2 \text{ A mm}^{-2}$  current density in the windings.

The above values will be used for preliminary work; finalization of the RF-section and interaction region magnet designs will require a more precise knowledge of the technical limitations and price-performance relationship of the power supplies, which our colleagues of the ISR-PO group are presently investigating.

For practical purposes,  $S_M$  and  $S_C$  will be selected among the currently available standards. A proposed set of design values appear in table 5 for lattice and RF-section magnets and in table 6 for interaction region magnets.

## 5. PROPOSED MAGNET DESIGNS

Having selected magnet geometry and coil current density, one is now able to put forward a preliminary design solution for orbit correction magnets.

Transverse cross-sections and calculated field quality of the proposed magnets appear in figs. 17 to 28, while their corresponding technical characteristics are listed in tables 7 and 8.

At this stage, further development work will be split into two parallel lines, namely:

- (i) More refined field calculations, in particular as concerns low field imperfections and three-dimensional effects at magnet ends.
- (ii) construction of prototypes, in order to assess technological problems and perform measurements (magnetic, electrical, thermal) permitting to check the calculations and finalize the design. The prototype magnets will also permit testing of prototype bi-polar power supplies, under construction in the ISR-PO group.

## ACKNOWLEDGEMENTS

It is a pleasure to acknowledge many helpful discussions with J-P. Gourber, G. Guignard and C. Wyss.

APPENDIX 1

Magnetic properties of non-oriented silicon steel  
as compared to low-carbon steel

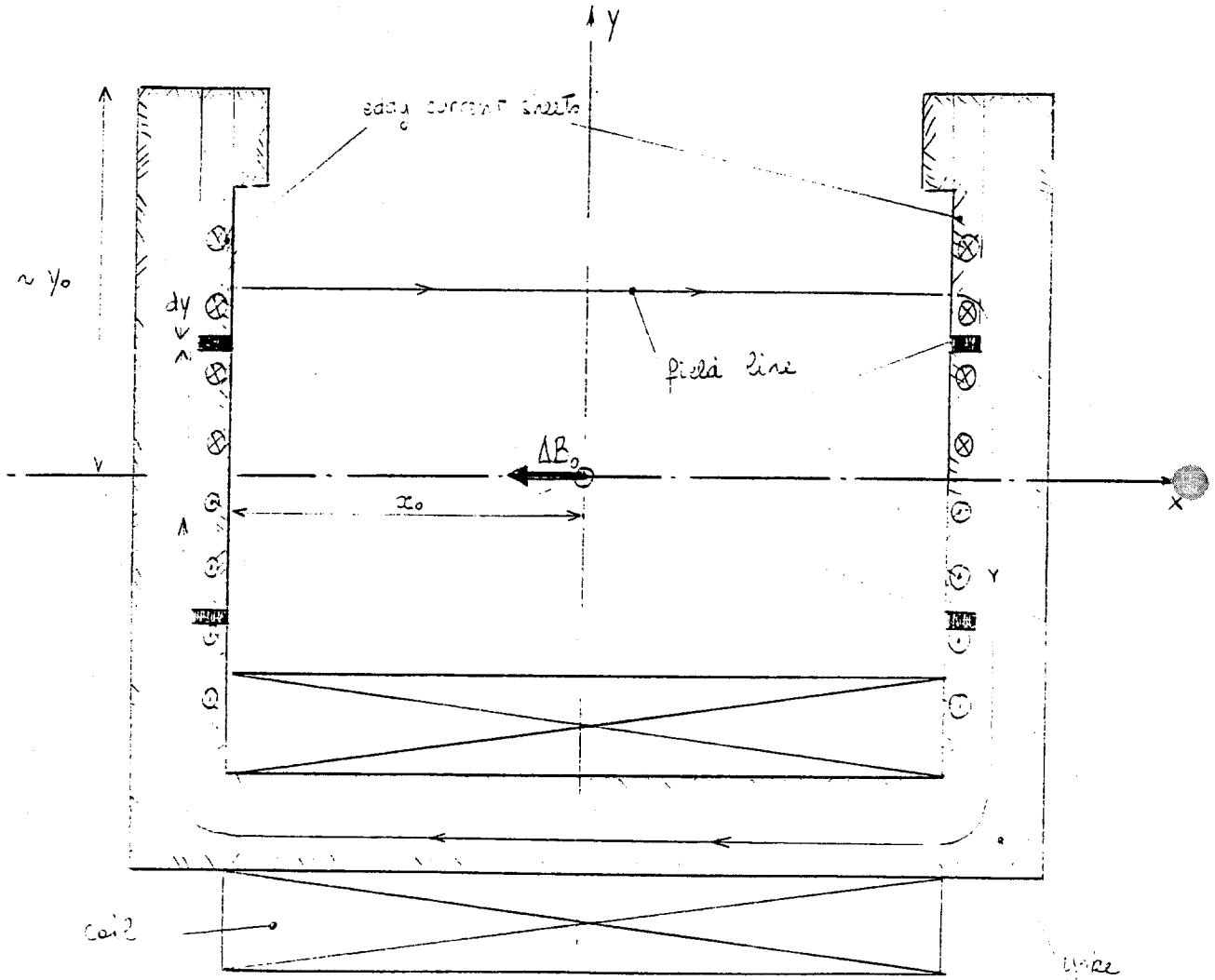
Silicon steels are used in place of low-carbon steels for AC electrotechnical applications in order to reduce AC losses associated with magnetic hysteresis. For LEP orbit correction magnets, which operate at low field levels, the coercive force of the material used for the magnetic circuit may produce a remanent field in the gap degrading the field quality and introducing a hysteresis effect having to be dealt with. One way of reducing this remanent field is to use a material with lower coercive force, provided other relevant magnetic properties remain acceptable.

Fig. 29 shows the variation of coercive force  $H_c$ , induction at saturation  $B_{sat}$  and maximum permeability  $\mu_{max}$  for non-oriented silicon steels, as a function of silicon content<sup>21)</sup>. While low-silicon grades do not seem to present any advantage over ISR low-carbon steel, high-silicon (i.e. 4.25% Si) steel allows gaining a factor of 2 on  $H_c$ , at the cost of a modest reduction in  $B_{sat}$ . Provided that plates of adequate thickness are available, the merits of silicon steel could be assessed in the course of prototype magnet work.

APPENDIX 2

Field error due to eddy currents in solid-cored magnets

The feasibility of solid-cored (instead of laminated) yokes for the orbit correction magnets depends primarily on the magnitude of the field error created by eddy current loops induced in the pole pieces upon ramping of the magnets; this field error should fall within the required tolerances on field quality, or at least be smaller than that created by the eddy current loops induced in the LEP vacuum chamber placed in the magnet gap. The order of magnitude of the field error can be assessed using the simple two-dimensional model below.



The local eddy current density  $\vec{J}$  occurring in the pole pieces of the magnet, of electrical resistivity  $\rho$ , is given by the Maxwell-Faraday relation:

$$\rho \text{rot } \vec{J} = - \frac{\partial \vec{B}}{\partial t}$$

In the eddy current sheets developing at the inner surface of each pole piece, this relation integrates into:

$$J_z = -\frac{1}{\rho} \frac{\partial B_z}{\partial t} y = - \frac{\dot{B}_0}{\rho} y$$

The eddy current density in the sheets increases linearly with distance from the centre of the pole piece, where it is zero for symmetry reasons.

Let  $e$  be the thickness of each eddy current sheet: although difficult to estimate,  $e$  is upperly bounded by the thickness  $d$  of the pole pieces. The steady-state field maps calculated (fig. 4) suggest that  $e \ll d$ ; in the following one shall take  $e = d/2$ .

The elementary current circulating in each loop at distance  $y$  from the centre is then:

$$dI = J_z dS = - \frac{\dot{B}_0 e}{\rho} y dy$$

The corresponding elementary field error produced by  $dI$  on the magnet axis can be calculated from Ampère's theorem:

$$d(\Delta B_0) = \frac{2 \mu_0 y dI}{\pi (y^2 + x_0^2)}$$

so that:

$$\Delta B_0 = \frac{2 \mu_0 \dot{B}_0 e}{\pi \rho} \int_0^{y_0} \frac{y^2 dy}{y^2 + x_0^2} = \frac{2 \mu_0 \dot{B}_0 e}{\pi \rho} \left( y_0 - x_0 \text{Arctan} \frac{y_0}{x_0} \right)$$

With the following numerical values:

$$\begin{aligned} B_0 &= 5 \times 10^{-4} \text{ T s}^{-1} \text{ (i.e. 1\% of } B_0 \text{ per second)} \\ e &= 10^{-2} \text{ m} \\ \rho &= 10 \times 10^{-8} \Omega \text{m (for low-carbon steel)} \\ x_0 &= y_0 = 10^{-1} \text{ m} \end{aligned}$$

one gets

$$B_0 \approx 10^{-6} \text{ T}$$

and

$$\Delta B_0 / B_0 \approx 2 \times 10^{-5}$$

This is well within the requirement of 1% setting accuracy; therefore it seems that a solid-cored construction is compatible with the ramping rate and field quality required for the orbit correction magnets. The use of silicon-steel for the yokes (see Appendix 1) would further reduce the amplitude of eddy currents, thanks to the higher electrical resistivity of the material.

APPENDIX 3

Cost Survey of DC Power Cables

In June 1981, eight major European cable manufacturers (listed below) were surveyed for fabrication standards and prices of DC power cables for the orbit correction magnets, on the basis of the specified characteristics below:

- conductor material: copper or aluminium
- cross-section: two-core, 1 to 6 mm<sup>2</sup>
- insulation, sheath: EPR, fire retardant.

No firm proposed aluminium conductors in this range of cross-sections for which the standard fabrications are 1, 1.5, 2.5, 4 and 6 mm<sup>2</sup>. The linear price to conductor cross-section relationship appears on fig. 30 which suggests a specific price of 30 to 35 SF per kg of copper in such finished cables, excluding installation. Most manufacturers are also able to supply multicore cables of such cross-sections as standard products, an option which may reduce installation costs.

- Alfacavi SpA, Via Serra 1, I - 15028 QUATTORDIO.
- BICC Ltd., 21 Bloomsbury Street, GB - LONDON WC 1B 3QN.
- Câbleries et Tréfileries SA de Cossonay, CH - 1305 COSSONAY-GARE.
- Câbles de Lyon SA, 170 ave. Jean Jaurès, F - 69353 LYON CEDEX 2.
- Fabrique Suisse d'Isolants, CH - 4226 BREITENBACH.
- Kabelmetal, Kabelkamp 20, D - 3000 HANNOVER 1.
- Pirelli SAPSA, Piazza Duca d'Aosta 3, I - 20124 MILANO.
- Thomson-Jeumont Câbles, 50 rue J.P. Timbaud, F - 92402 COURBEVOIE.

APPENDIX 4

Economic incidence of power supply maximum output voltage

Minimizing the total mass of copper in the cable + coil system of an orbit correction magnet is achieved by taking the current densities in coil and cable such that:

$$\begin{cases} j_M = \frac{U}{2\rho\sqrt{l_c l_c^*}} \\ j_c = \frac{U}{2\rho l_c} \end{cases}$$

The corresponding mass of copper is

$$m^{opt} = m_M^{opt} + m_c^{opt} = \frac{4\mu\rho^2 NI}{U} \sqrt{l_c l_c^*}$$

Figs. 31 and 32 show the variations of  $j_c^{opt}$ ,  $j_M^{opt}$  and  $m^{opt}$  as a function of  $U$  for lattice corrector magnets. The present design value of 120 V leads to relatively low current densities in coil and cable, and hence a large mass of copper (about 100 kg per unit). Upgrading the maximum output voltage to, say, 180 V, would probably raise no extra requirement on electrical insulation; above all, it would reduce by a factor of 1.5 the amount of copper required, while still allowing acceptable current densities in coil and cable.

The corresponding capital savings have to be put in balance with the associated increased cost of the power supply. Present trends in semiconductor device development lead our colleagues of the ISR-PO group to believe that power supply output voltage could be increased, whilst still maintaining necessary safety margins; development work will continue in this direction.

REFERENCES

1. A. Hutton, 'Parameter list for LEP version 11', LEP Note 289, 9th March 1981.
2. G. Guignard, 'Closed orbit monitoring and correction in LEP version 11', LEP Note 306, 9th June 1981.
3. 'Design study of a 22 to 130 GeV  $e^+e^-$  colliding beam machine (LEP)', CERN/ISR-LEP/79-33, 22nd August 1979 (The Pink Book).
4. O. Gröbner, private communication.
5. O. Gröbner and C. Wyss, 'Vacuum chamber cross-section and diameter of the inscribed circle in the quadrupole and sextupole magnets', LEP Note 319, 9th September 1981.
6. G. Bachy et al., 'LEP service areas', LEP Note 312, 29th June 1981.
7. A.M. Winslow, 'Numerical solution of the quasilinear Poisson equation in a non-uniform triangle mesh', Journ. Comput. Phys. 2, 149-172 (1967).
8. J.P. Gourber and L. Resegotti, 'Implication of the low field levels in the LEP magnets', Proc. 1979 Particle Accelerator Conference, March 1979.
9. Norme NF A 46-012, February 1973.
10. DIN 1540 (April 1970) and 1543 (July 1959).
11. H. Hsieh (BNL), private communication.
12. R.J. Noyes, 'Busbars or cables for LEP lattice lenses', Internal Note, ISR-BOM/RJN/ml, 7th May 1981.
13. W. Richter, 'Cooling system for LEP', LEP Note 311, 19th June 1981.
14. G. Guignard, private communication.
15. H. Isch, private communication.
16. J. Pett, private communication.
17. C. Wyss, private communication.
18. L. Weil, 'Éléments des échanges thermiques', Gauthier-Villars, Paris 1965.
19. Notice 'Le Fil Dynamo', 1981.
20. W. Richter, private communication.
21. R.M. Bozorth, 'Ferromagnetism', Van Nostrand, Princeton, 1964.
22. R. Forrest, private communication.
23. C. Roy, LEP Note to be published.

- Table 1 : Basic requirements for orbit correction magnets -

Magnet type	Number of units	gap (mm)	Max. field (Tesla)	Horiz. apert. (mm)	Vertic. apert. (mm)
CV lattice	176	200	0.04	$\pm 25$	$\pm 33$
CH lattice	176	100	0.07	$\pm 59$	$\pm 14$
CV <sub>RF</sub>	80	200	0.05	$\pm 25$	$\pm 33$
CH <sub>RF</sub>	64	120	0.10	$\pm 59$	$\pm 14$
CVI	16	180	0.16	$\pm 63$	$\pm 61$
CHI	16	180	0.10	$\pm 71$	$\pm 37$

- Table 2 : Longitudinal position of orbit correction magnets -

Half-octant close to short interaction region ( 2, 4, 6, 8 )	
Magnet type	D. from interact. point (m)
CVI	10.8
CHI	16.6
CV	66.1
CH	78.7
CV	103.0
CV	151.5
CH	175.5
CH	224.2
CV	248.5
CV	302.7
CH	329.7
CH	403.8
CV	443.3
CV	522.3
CH	561.8
CH	640.8
CV	680.3
CV	759.3
CH	799.8
CH	877.8
CV	917.3
CV	996.3
CH	1035.8
CH	1114.8
CV	1154.3
CV	1233.3
CH	1272.8
CH	1351.8
CV	1391.3
CV	1470.3
CH	1509.8
CH	1588.8
CV	1628.3

Half-octant close to long interaction region ( 1, 3, 5, 7 )	
Magnet type	D. from int. point (m)
CVI	15.8
CHI	20.1
CV	62.3
CH	74.9
CV	99.2
CV	147.7
CH	172.0
CH	220.4
CV	244.7
CV	298.9
CH	326.0
CH	400.2
CV	438.5
CV	519.1
CH	558.6
CH	637.6
CV	677.1
CV	756.1
CH	795.6
CH	874.6
CV	914.1
CV	993.1
CH	1032.6
CH	1111.6
CV	1151.1
CV	1230.1
CH	1269.6
CH	1348.6
CV	1388.1
CV	1467.1
CH	1506.6
CH	1585.6
CV	1625.1

Table 3 : Comparative study of magnet geometries -

Magnet geometry	Pole-and- return-yoke	Window-frame, racetrack coils	Window-frame, bedstead coils	Horseshoe
Overall length (cm)	52	44	60	44
Overall width (cm)	34	24	28	24
Overall height (cm)	40	25	20	22.5
$\tilde{j}_{\text{coil}}$ (A.cm <sup>-2</sup> )	200	200	200	200
$j_{\text{conductor}}$ (A.cm <sup>-2</sup> )	250	250	250	250
$B_{\text{max}}$ in yoke (Tesla)	1.02	0.43	0.31	1.29
$m_{\text{yoke}}$ (kg)	136	50	50	39
$m_{\text{coil}}$ (kg)	43	52	43	26
$m_{\text{total}}$ (kg)	179	102	93	65
Max. power (W)	550	660	550	330
Max. stored energy (J)	48	25	13	24

Table 4 : Optimized design values for CH and CV magnets, under the condition  $U_{max} = 120$  V.

Magnet type	CV <sub>l</sub>	CH <sub>l</sub>	CV <sub>RF</sub>	CH <sub>RF</sub>
(NI) (A.turns)	6370	5570	7960	9550
$l_c^*$ (m)	2210	2200	520	580
$l_c$ (m)	3480	3400	830	880
$j_M^{opt}$ (A.cm <sup>-2</sup> )	120	122	507	467
$j_c^{opt}$ (A.cm <sup>-2</sup> )	96	98	402	379
I (A)	2.3	2.0	12.1	13.4
N (turns)	2770	2785	657	714
$S_M^{opt}$ (mm <sup>2</sup> )	1.9	1.7	2.4	2.9
$S_c^{opt}$ (mm <sup>2</sup> )	2.4	2.1	3.0	3.5
$m_c^{opt} = m_M^{opt}$ (kg)	47	41	14	18
$m_{total}$ (kg)	94	82	28	36
$P_M$ (W)	140	120	730	800

- Table 5 : Design values for CH and CV magnets -

Magnet type	CV <sub>e</sub>	CH <sub>e</sub>	CV <sub>RF</sub>	CH <sub>RF</sub>
Ni (A.turns)	6370	5570	7960	9550
$l_c^*$ (m)	2210	2200	520	580
$l_c$ (m)	3480	3400	830	880
$j_M^{\text{design}}$ (A.cm <sup>-2</sup> )	125	145	293	271
$j_c^{\text{design}}$ (A.cm <sup>-2</sup> )	100	103	180	218
I (A)	2.5	2.6	4.5	5.5
N (turns)	2540	2160	1770	1760
$S_M^{\text{design}}$ (mm <sup>2</sup> )	2.010	1.767	1.539	2.010
$S_c^{\text{design}}$ (mm <sup>2</sup> )	2.5	2.5	2.5	2.5
$m_M$ (kg)	45	34	24	31
$m_c$ (kg)	49	49	12	13
$m_{\text{total}}$ (kg)	94	83	36	44
$P_M$ (W)	140	150	420	470

Table 6 : Design values for CHI and CVI magnets -

Magnet type	CVI	CHI
NI (A.turns)	22920	14330
$l_c^*$ (m)	125	130
$l_c$ (m)	125	130
$j_M^{\text{design}}$ (A.cm <sup>-2</sup> )	170	236
$j_c^{\text{design}}$ (A.cm <sup>-2</sup> )	240	240
I (A)	6.0	6.0
N (turns)	3820	2390
$S_M^{\text{design}}$ (mm <sup>2</sup> )	3.529	2.544
$S_c^{\text{design}}$ (mm <sup>2</sup> )	2.5	2.5
$m_M$ (kg)	120	54
$m_c$ (kg)	2.8	2.9
$m_{\text{total}}$ (kg)	123	57
$P_M$ (W)	700	610

Table 7 : Characteristics of CV and CH magnets -

Magnet type	CV <sub>2</sub>	CH <sub>2</sub>	CV <sub>RF</sub>	CH <sub>RF</sub>
Length (cm)	49	54	47	51
Width (cm)	24	36	24	34
Height (cm)	27	16	25	18
m <sub>yoke</sub> (kg)	42	103	48	70
m <sub>coil</sub> (kg)	45	34	24	31
m <sub>magnet</sub> (kg)	87	137	72	101
N (turns)	2540	2160	1770	1760
i (A)	2.5	2.6	4.5	5.5
R <sub>20°C</sub> (Ω)	23.	22.	21.	15.
L (H)	10.	16.	5.1	4.5
P (W)	140	150	420	470
D* (l min <sup>-1</sup> )	0.10	0.11	0.30	0.34

\* Cooling water flow required, allowing T<sub>out</sub> - T<sub>in</sub> = 20°C.

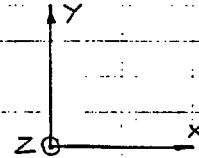
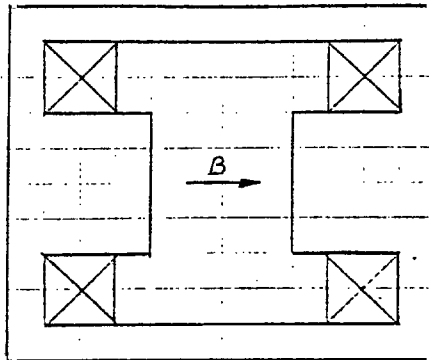
Table 8 : Characteristics of CVI and CHI magnets -

Magnet type	CVI	CHI
Length (cm)	62	50
Width (cm)	26	37
Height (cm)	52	24
$m_{yoke}$ (kg)	148	89
$m_{coil}$ (kg)	120	54
$m_{magnet}$ (kg)	268	143
N (turns)	3820	2390
$I$ (A)	6.0	6.0
$R_{20^{\circ}C}$ ( $\Omega$ )	23	17
L (H)	32	12
P (W)	700	610
$D^*$ ( $l \cdot min^{-1}$ )	0.50	0.44

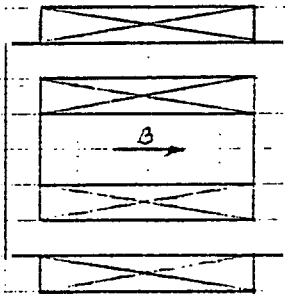
\* Cooling water flow required, allowing  $T_{out} - T_{in} = 20^{\circ}C$

Figure 1: Two-dimensional magnet geometries studied.

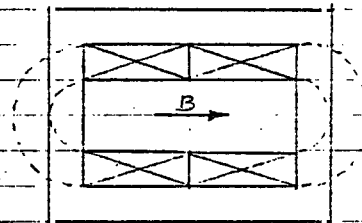
1. Conventional "pole-and-return-yoke"



2. "Window-frame"

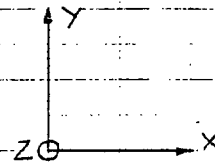
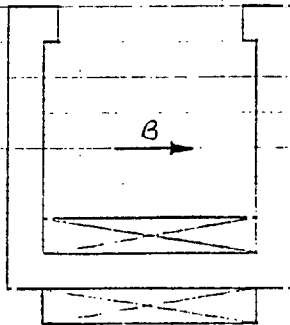


(a) racetrack coils



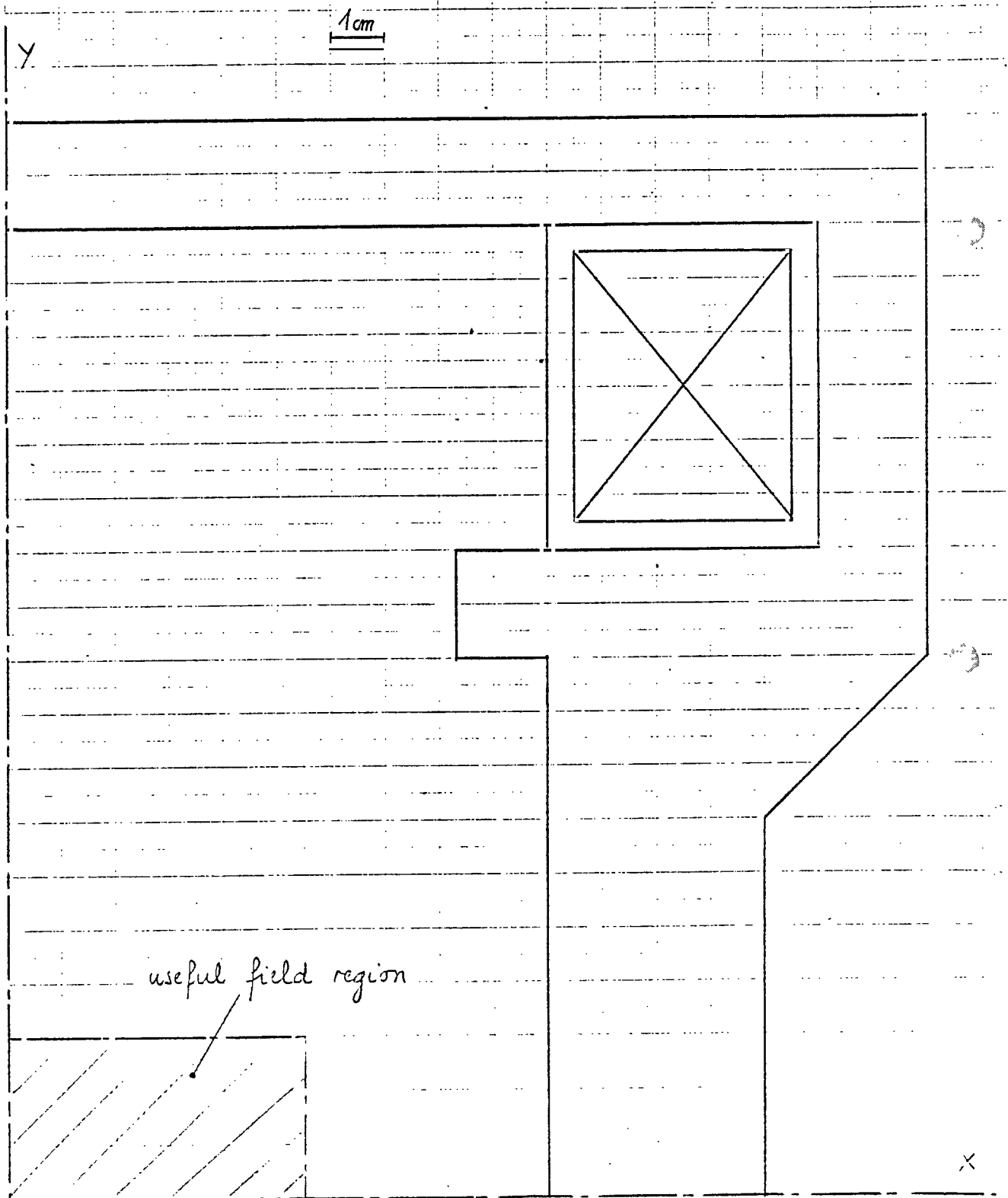
(b) beaded coils

3. "Horseshoe"

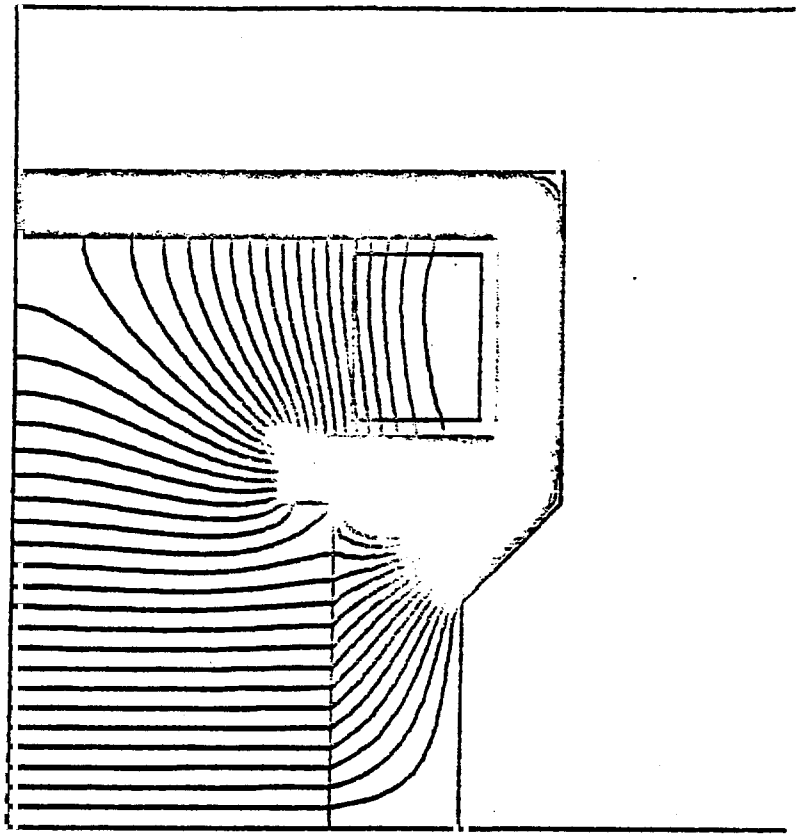


- Figure 2: Conventional "pole-and-return-yoke"  
geometry magnet.

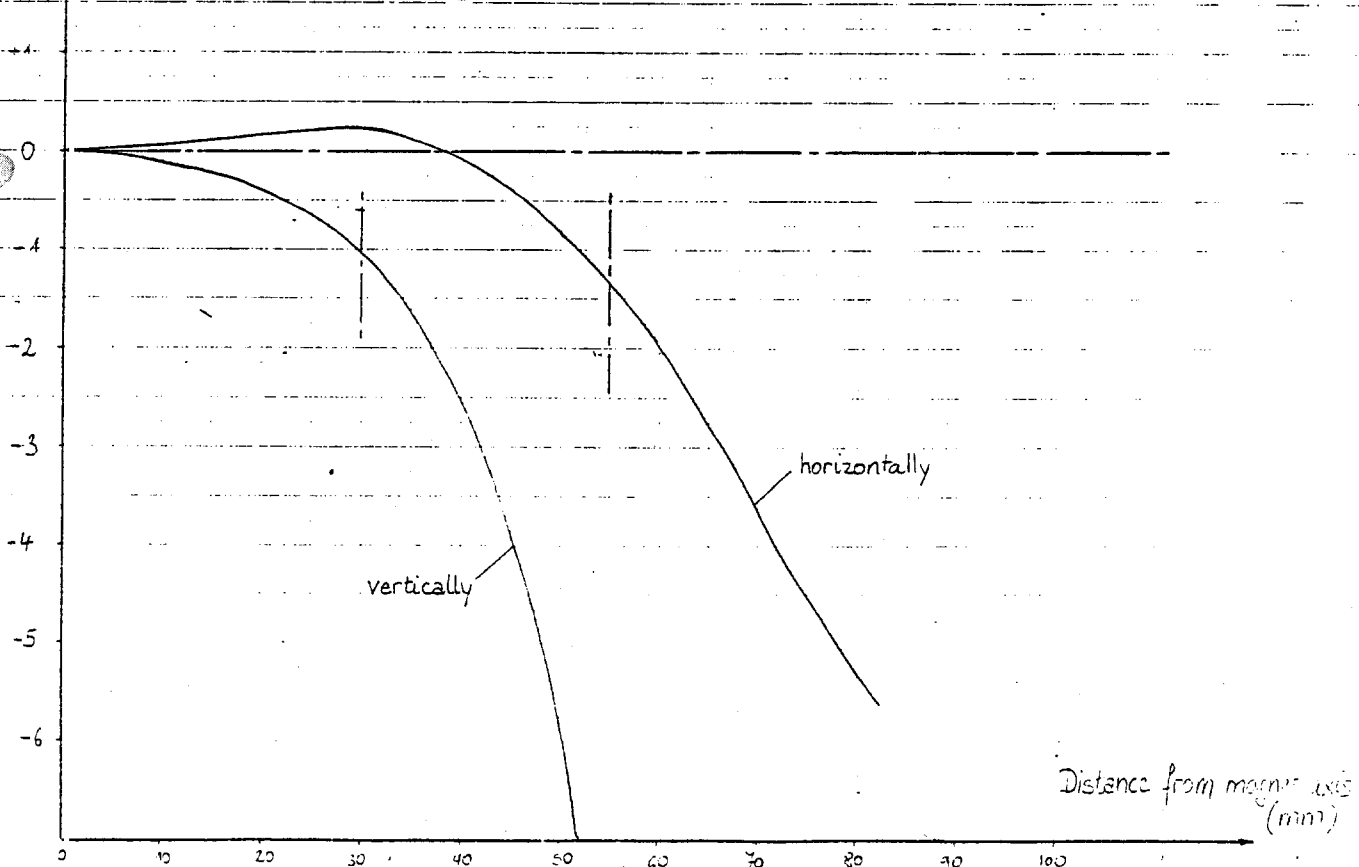
2.a. Transverse cross-section (scale 1:1)



2.b. Magnetic field calculations



Field relative inhomogeneity (%)



scale 1:1

1cm

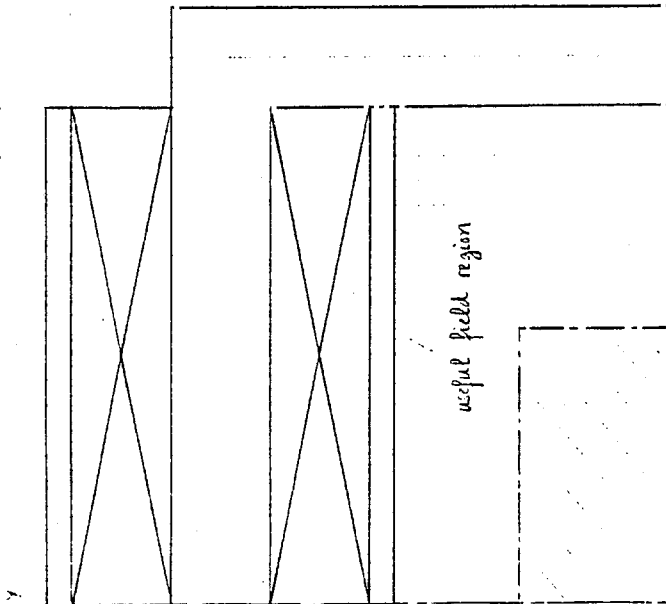


Figure 3:

"Window-frame" geometry magnet

• Race-track coils →

x

• Bedstead coils →

Field relative inhomogeneity (%)

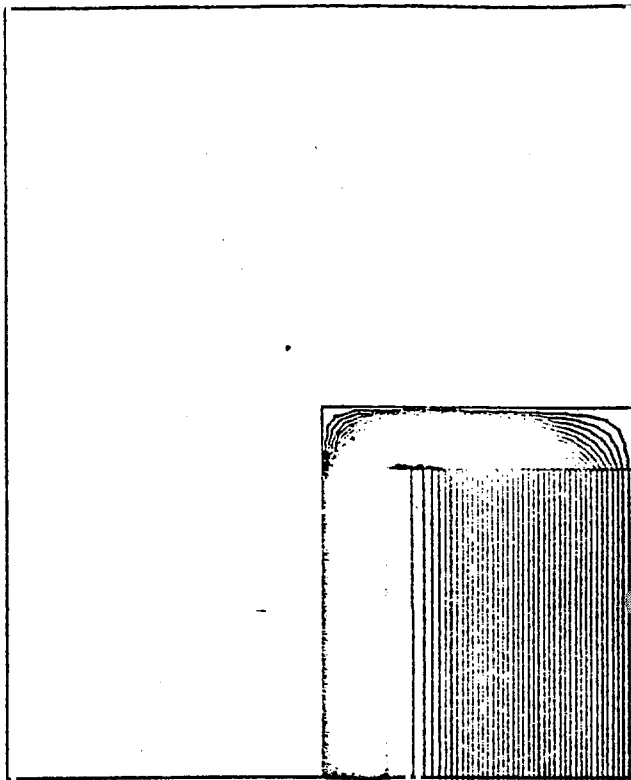
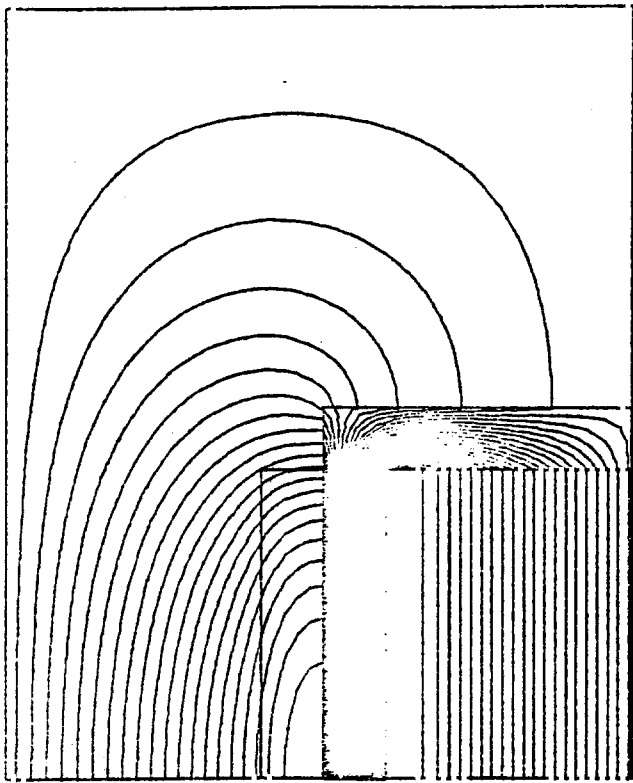
+2  
+1  
-1  
-2  
0

vertically

horizontally

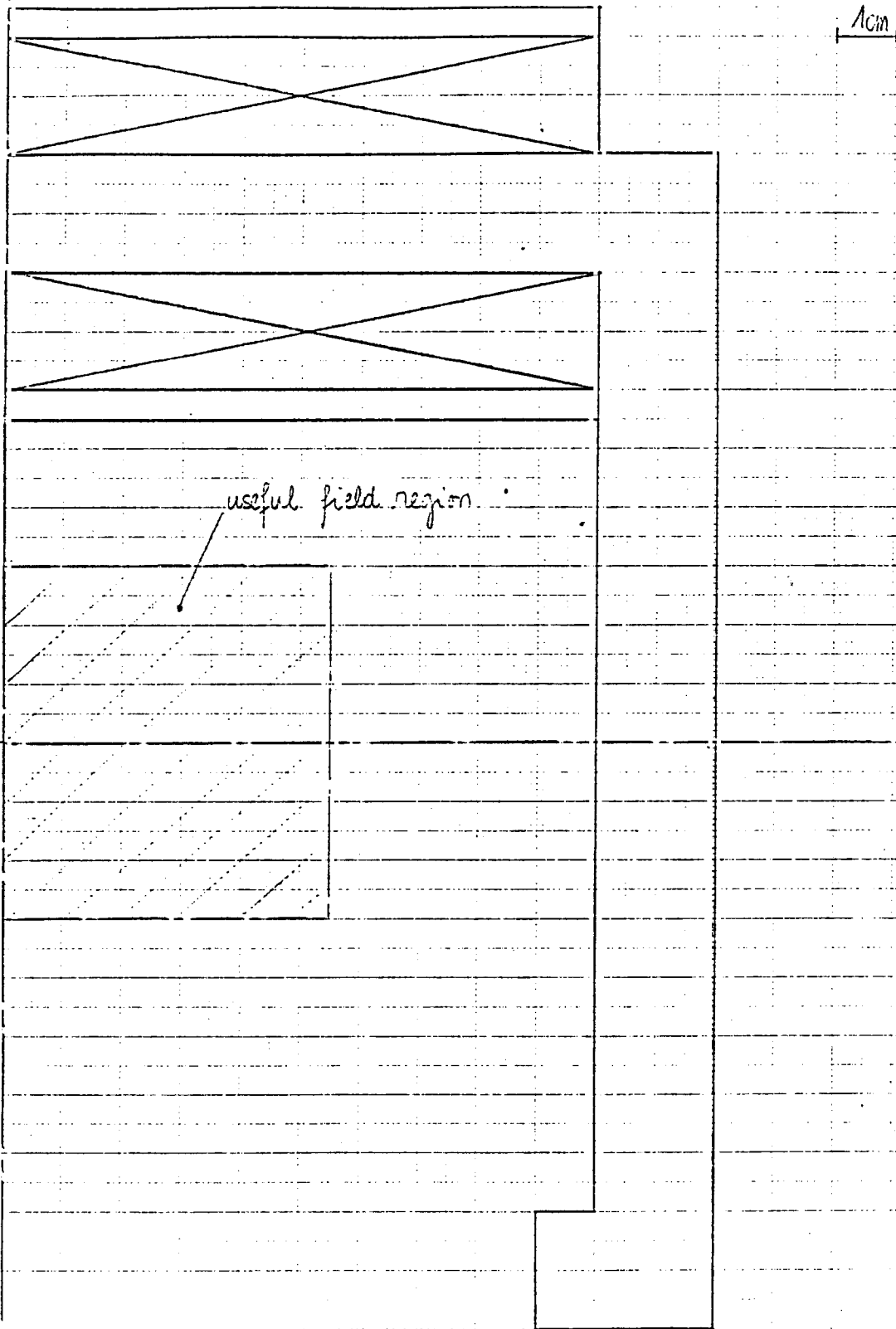
Distance from magnet axis (mm)

0 10 20 30 40 50 60 80

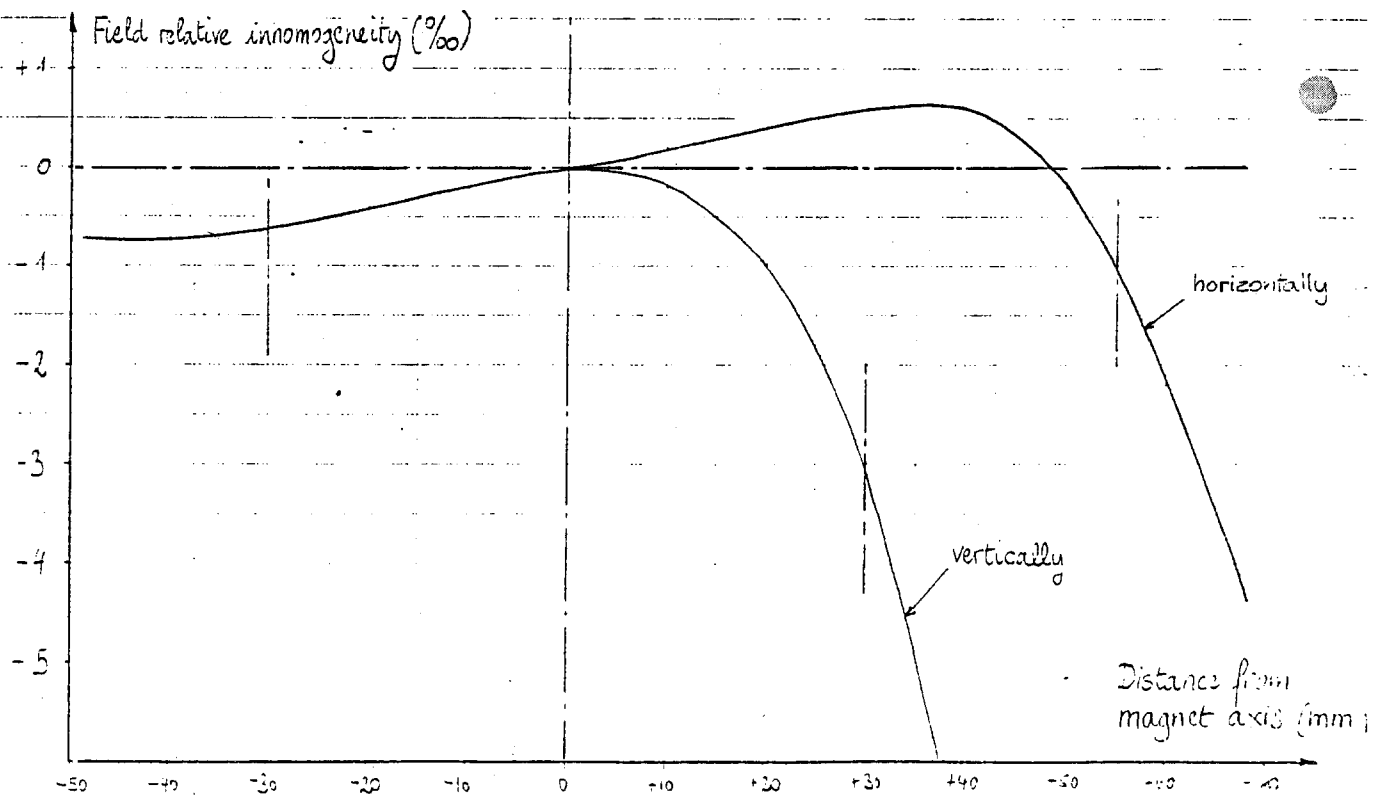
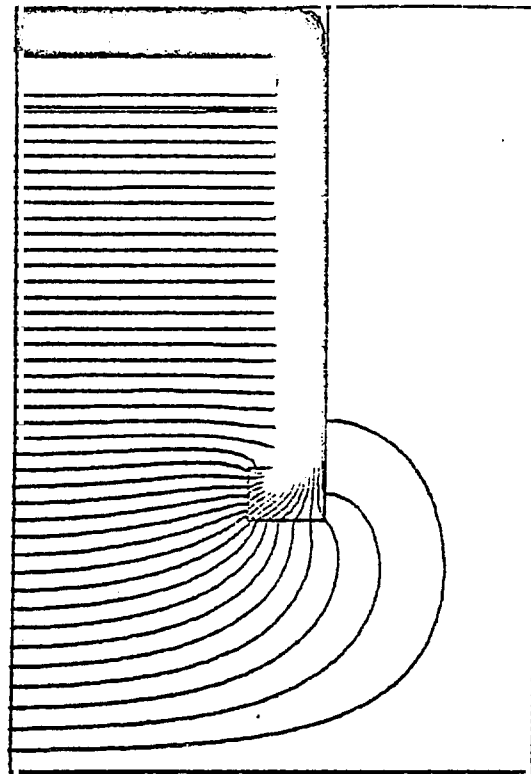


- Figure 4: "Horseshoe" geometry magnet:

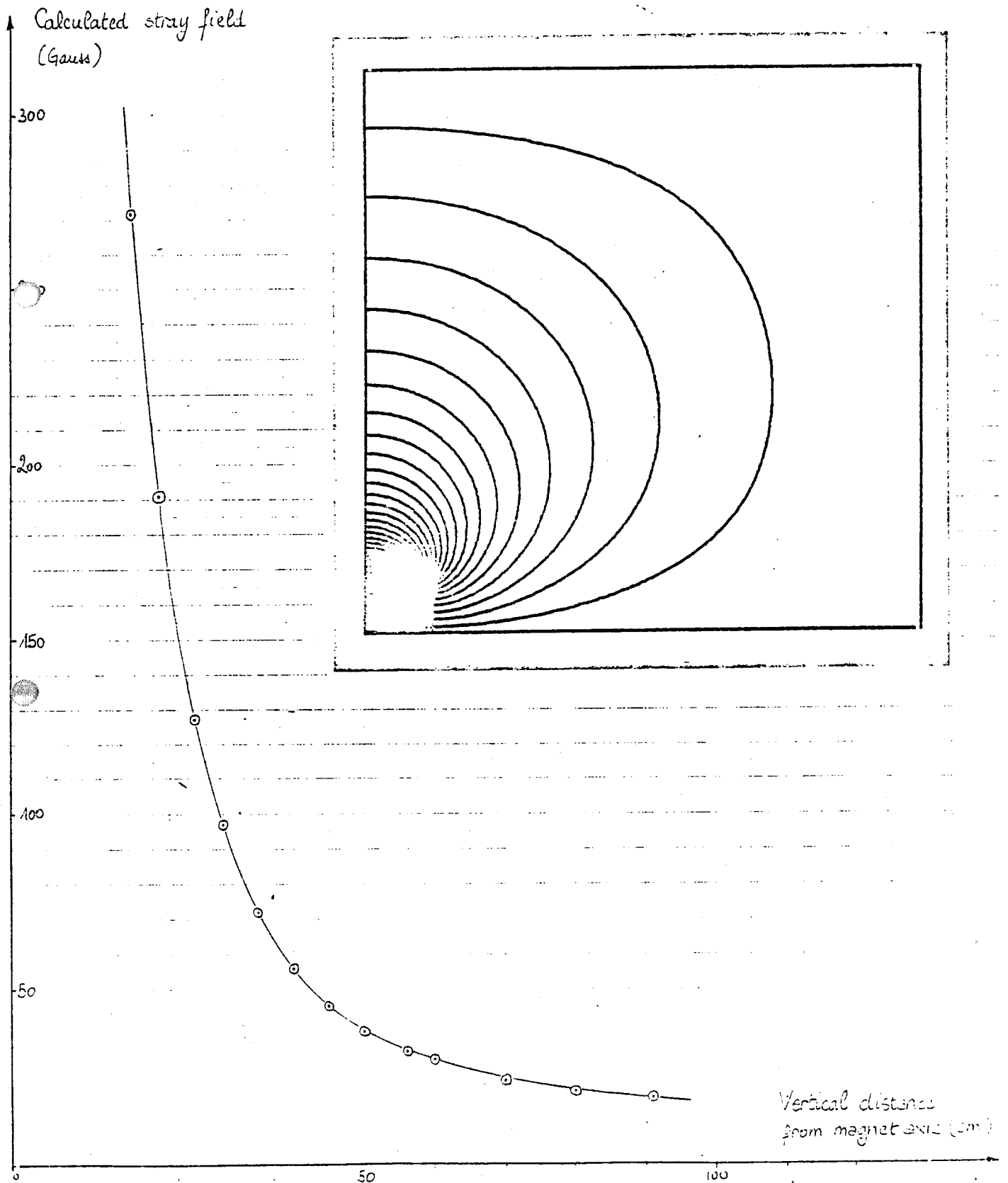
4.a. Transverse cross-section (scale 1:1)



# 4.b. Magnetic field calculations



-Figure 5: Calculated stray field in symmetry plane of horseshoe magnet-



- Figure 6 : Relative permeability of 15R-steel -

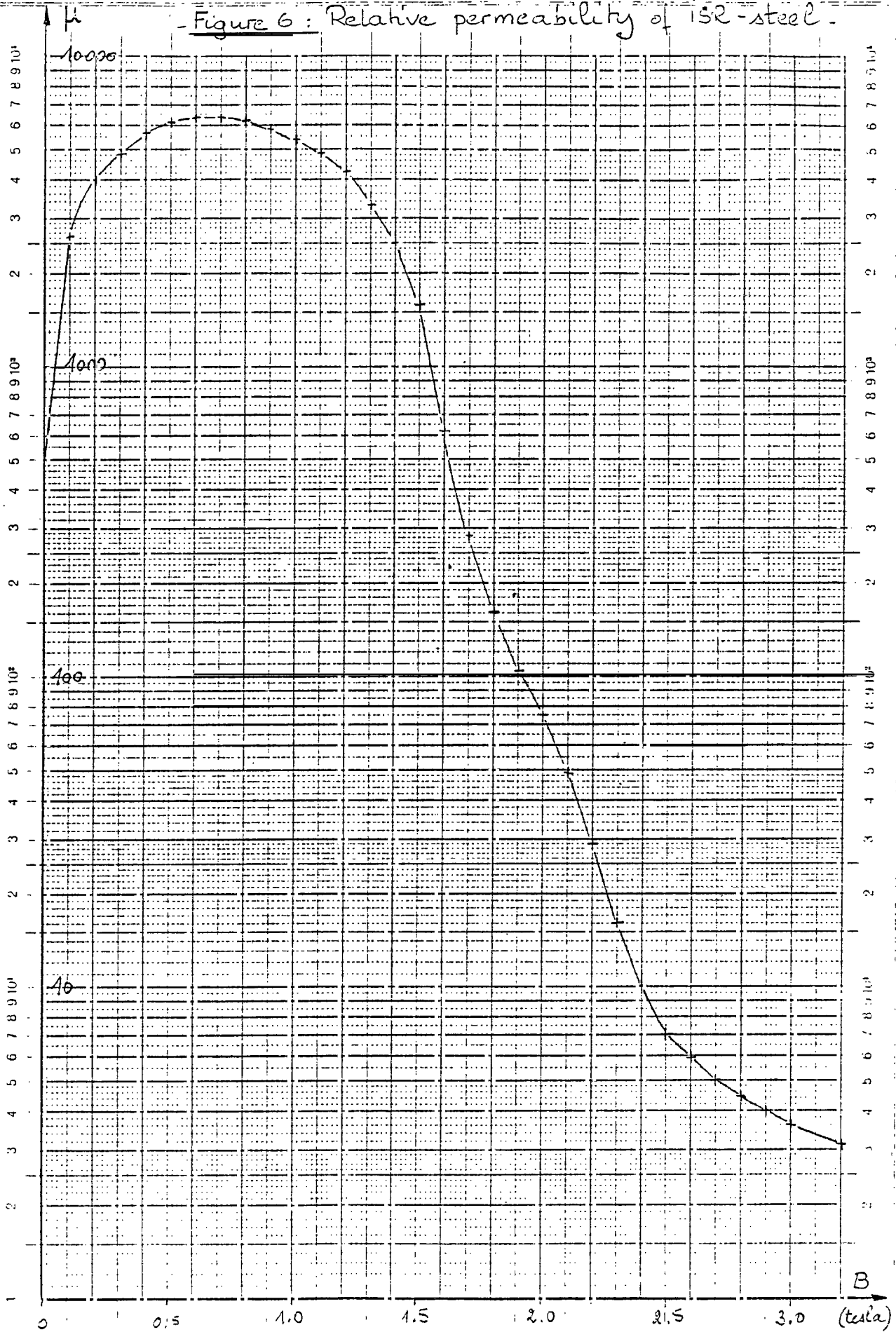
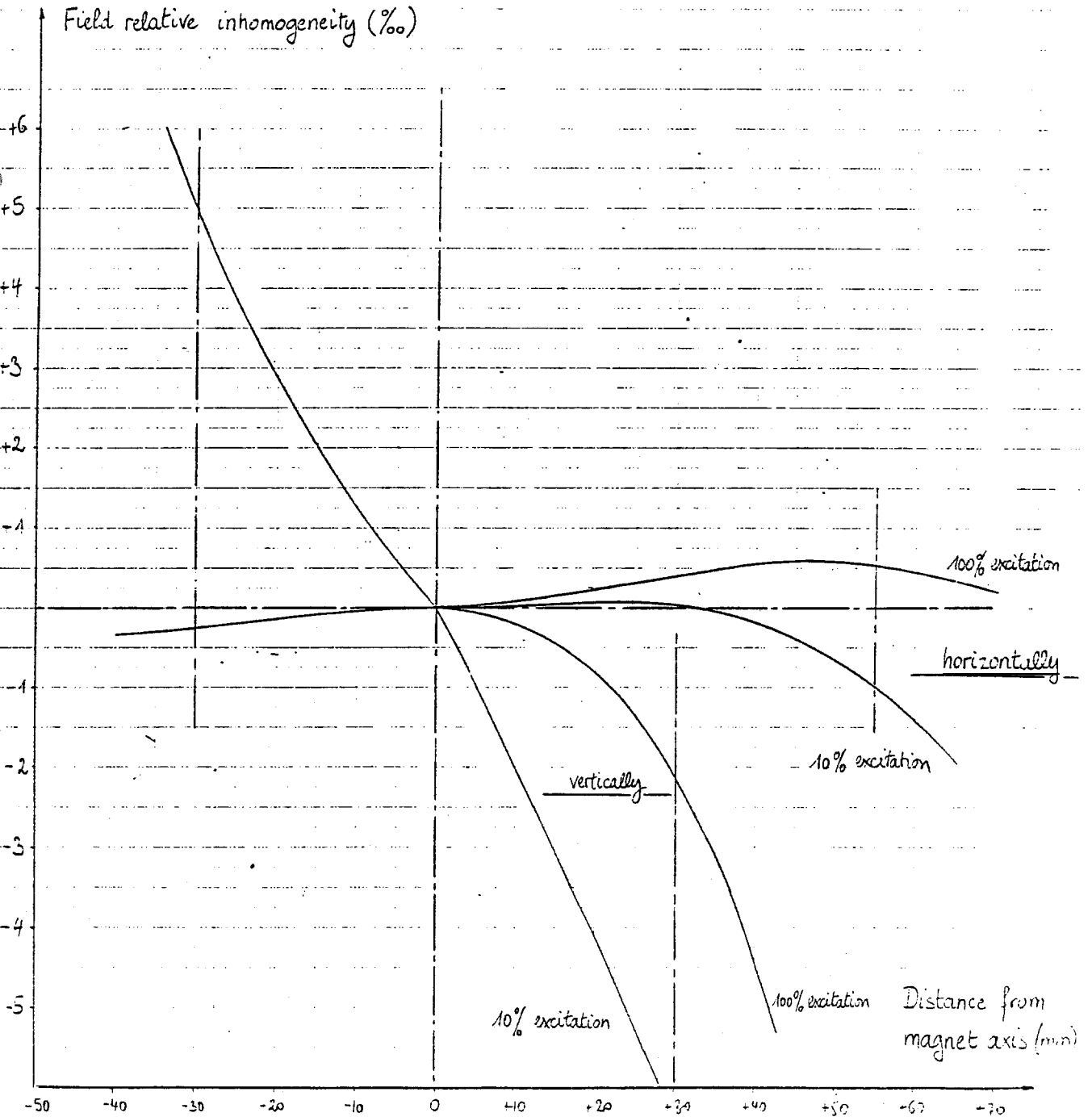


Figure 7: Degradation of field quality at low excitation, due to low- $\mu$  effect, horseshoe magnet.



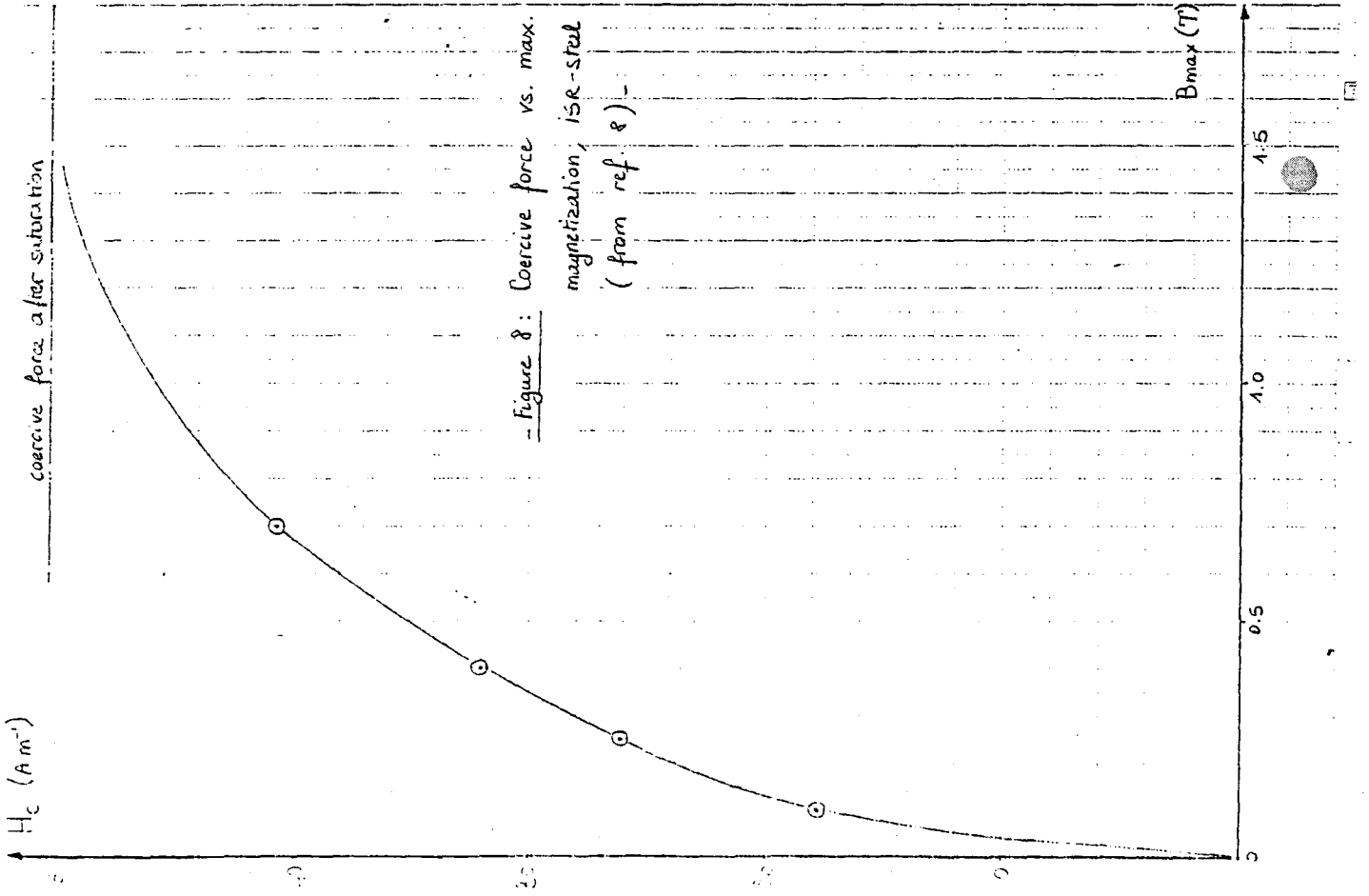


Figure 9: Calculated remanent central field in horizontal magnet vs. pole thickness, after max. excitation.

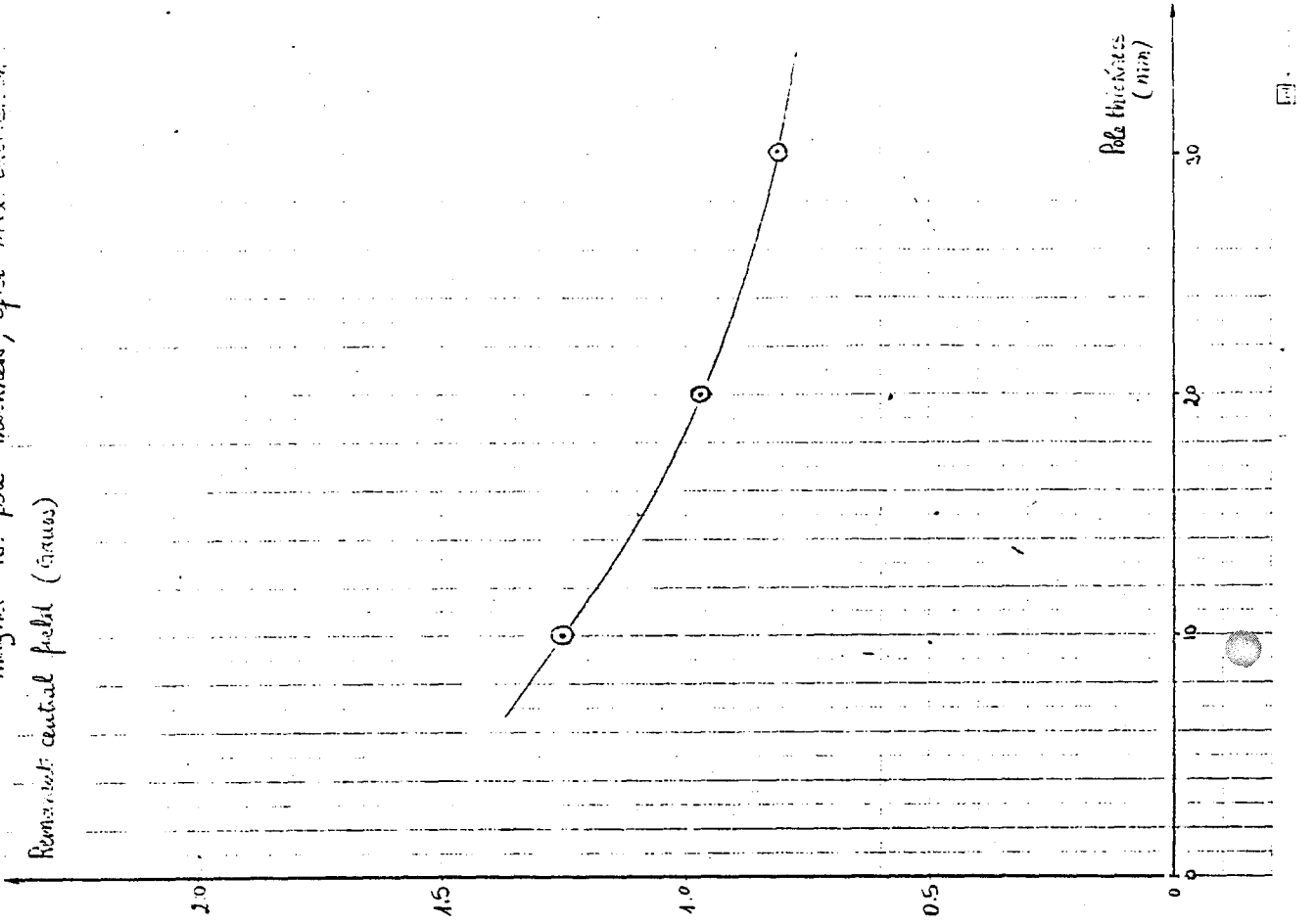


Figure 10: Compensation of field error due to coil insulation and tolerances, by small shoulder in pole piece.

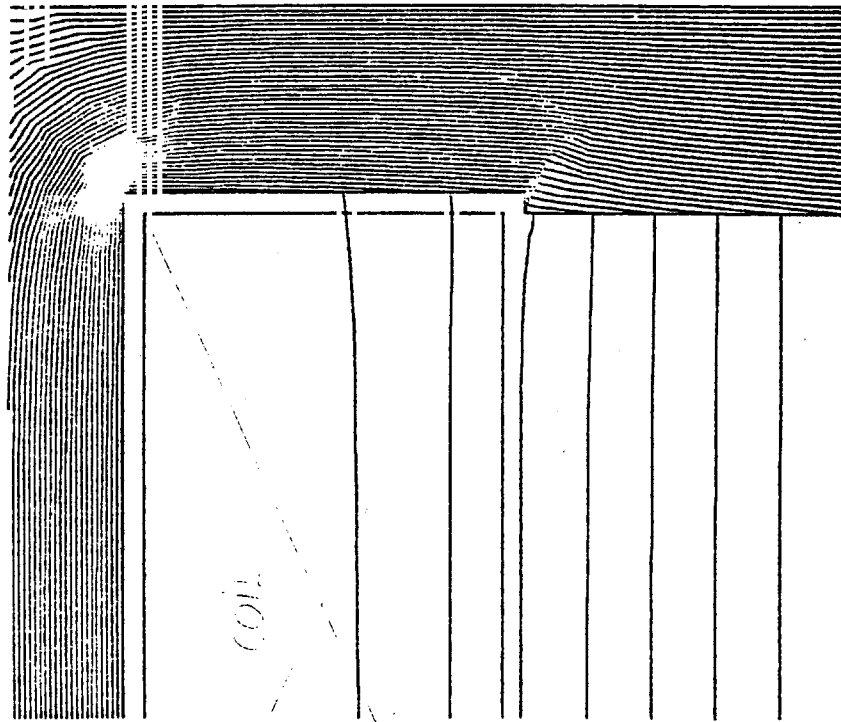


Figure 11: Filling factor vs. wire cross-section for coils wound with enamelled grade 2 round wire (from ref. 19)

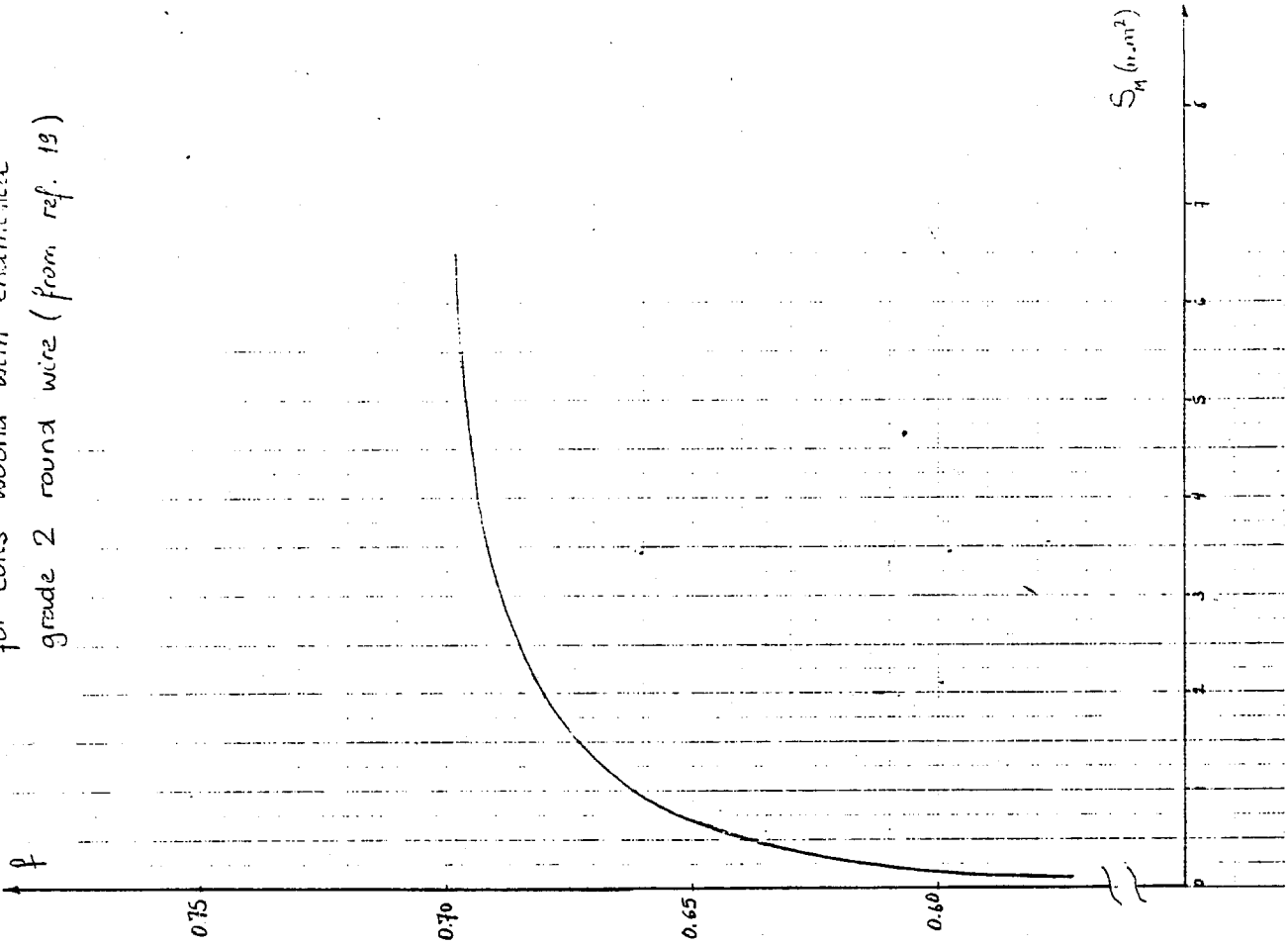


Figure 12: Equivalent thermal conductivity ratio of coil wound with round wire vs. filling factor (from ref. 18)

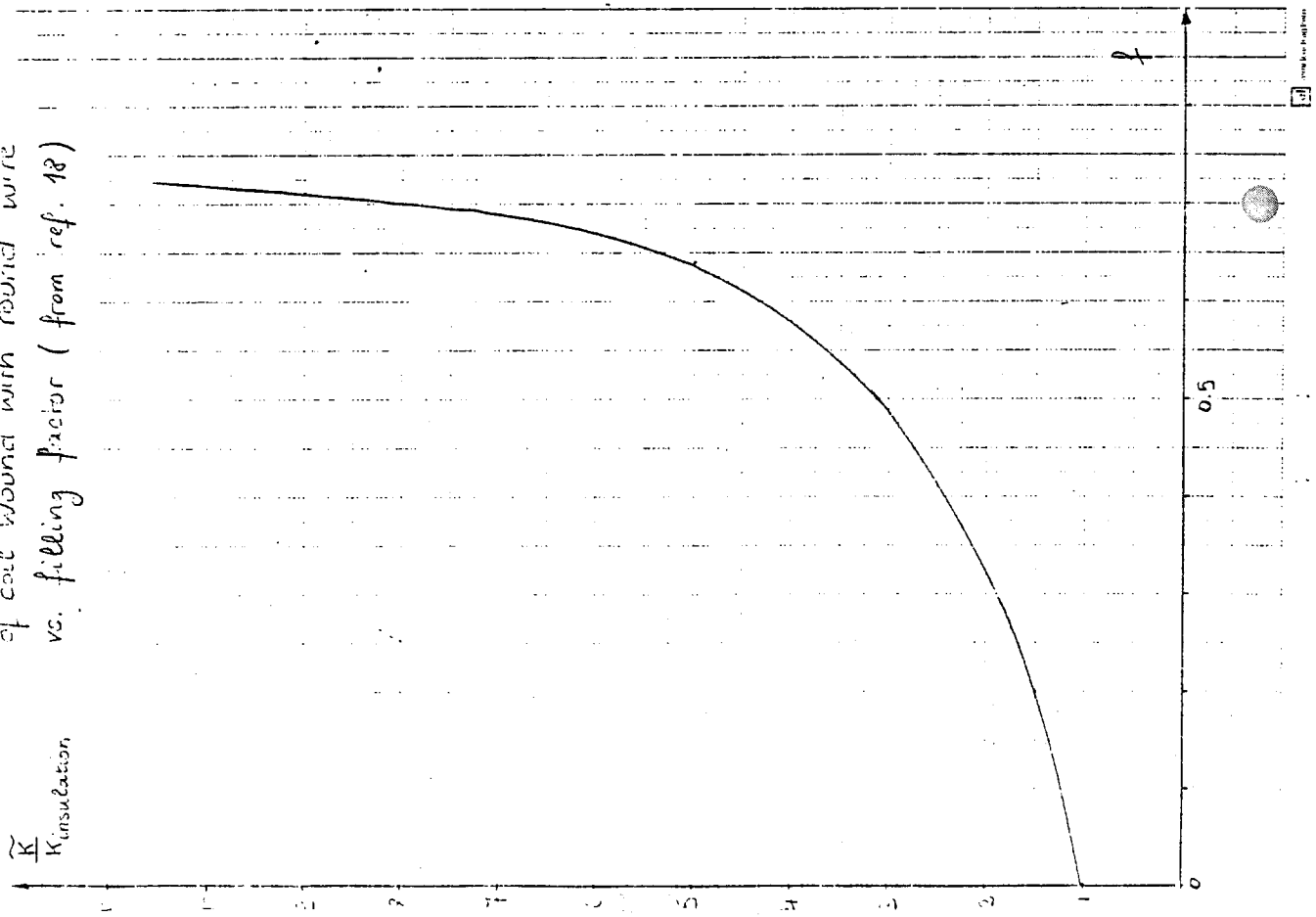
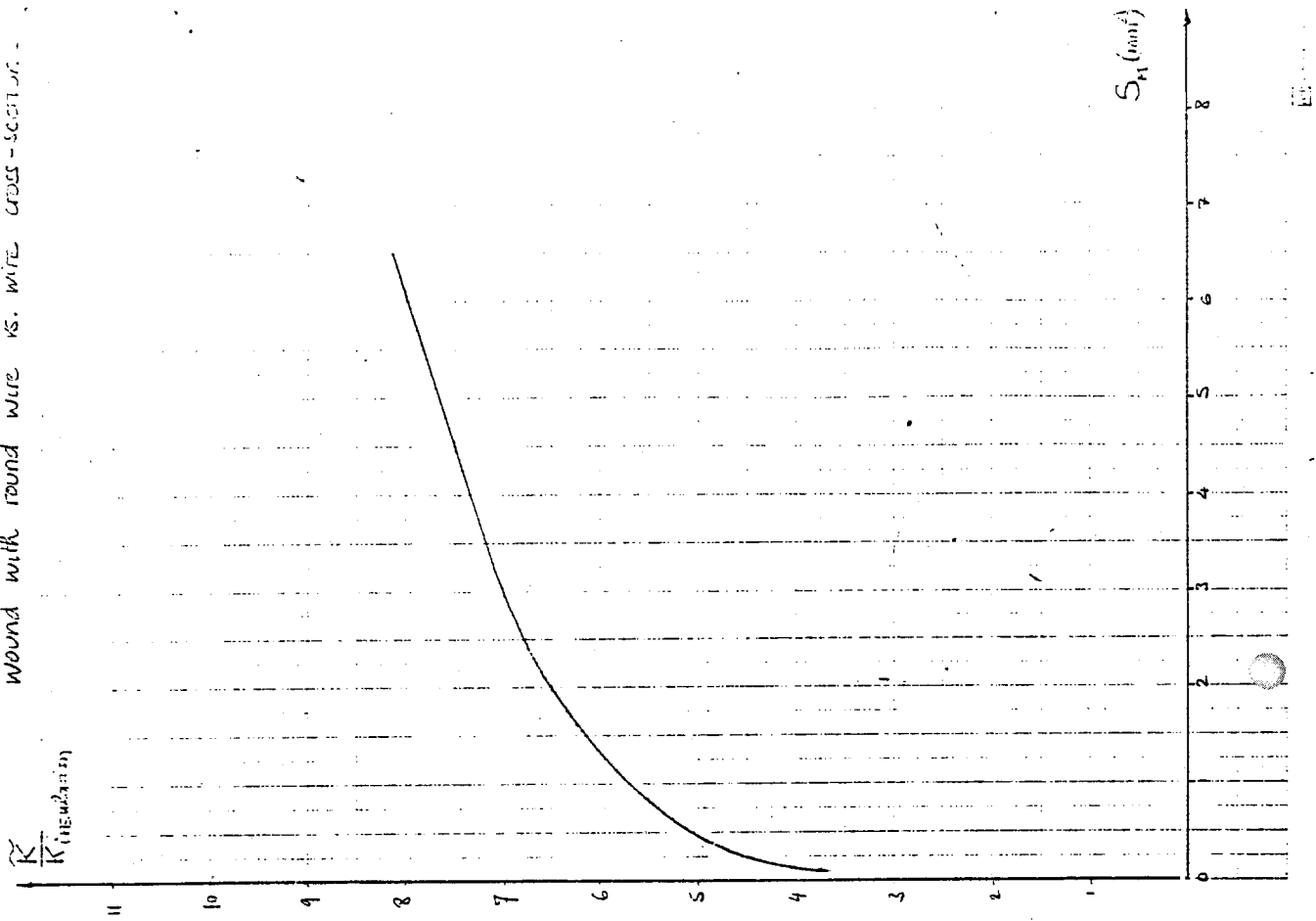
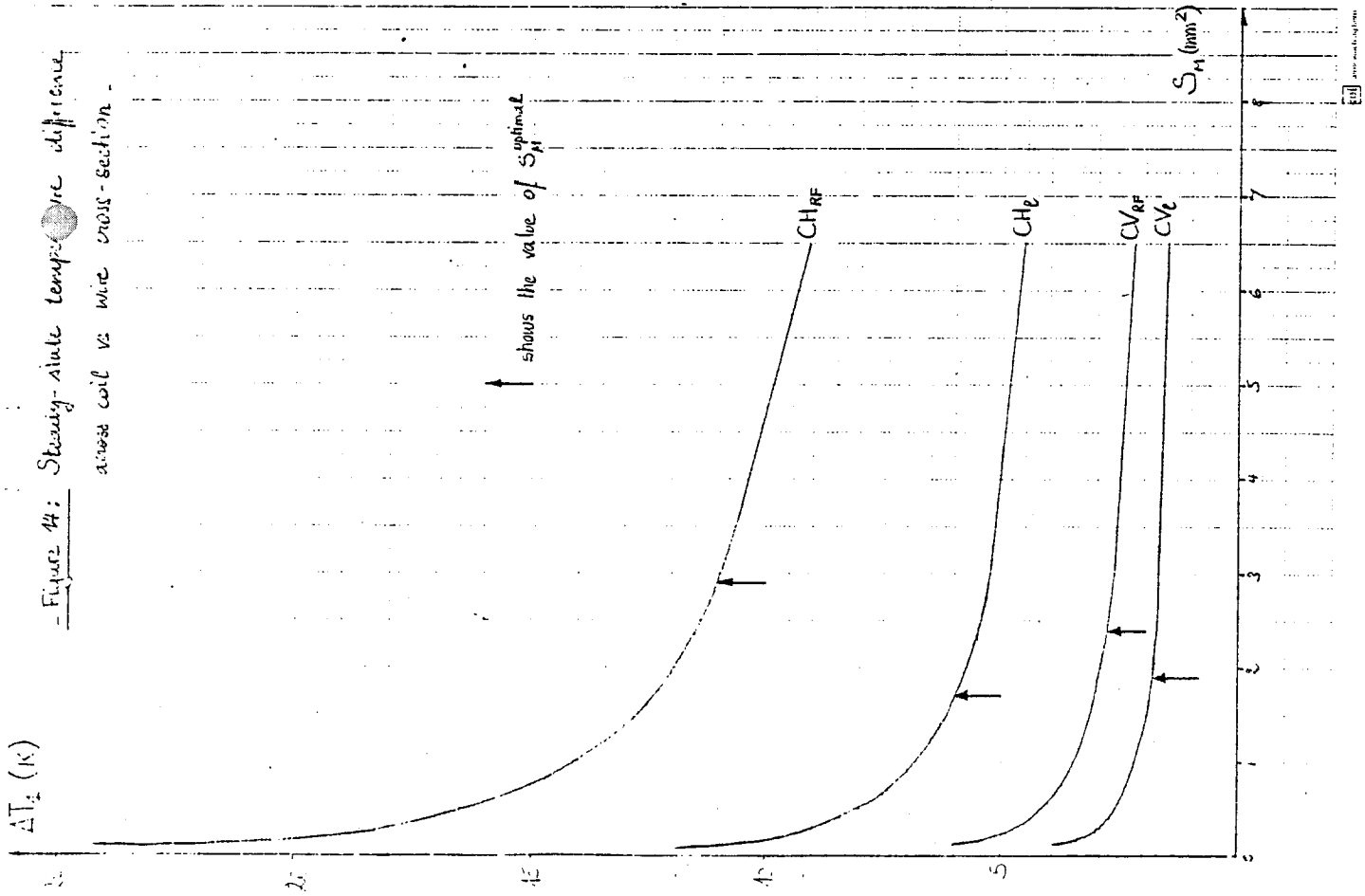


Figure 13: Equivalent thermal conductivity ratio of coil wound with round wire vs. wire cross-section.



- Figure 4: Steady-state temperature difference vs wire cross-section -



- Figure 15: Steady-state temperature difference at coil surface vs. current density in conductor, air-cooling.

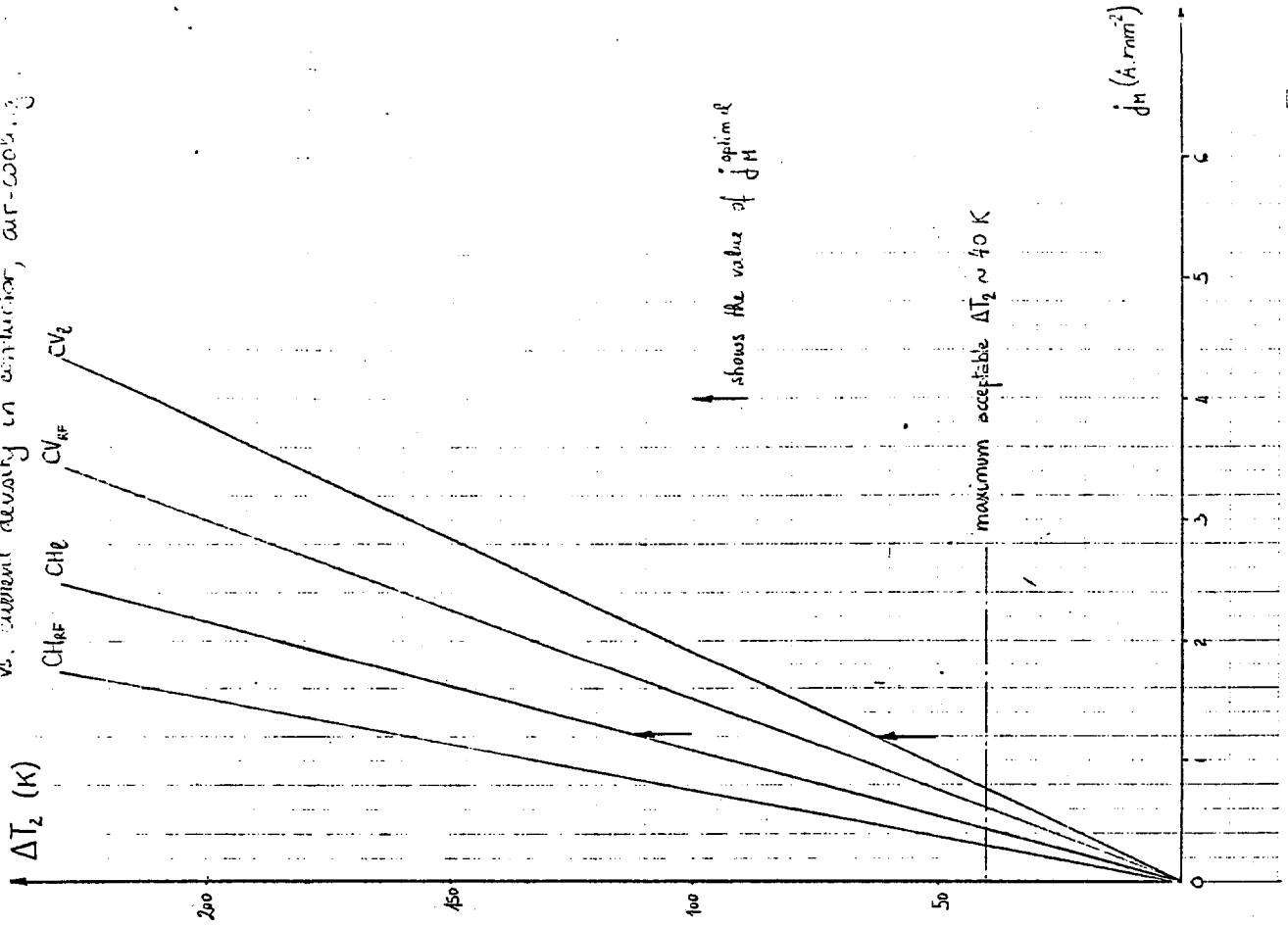
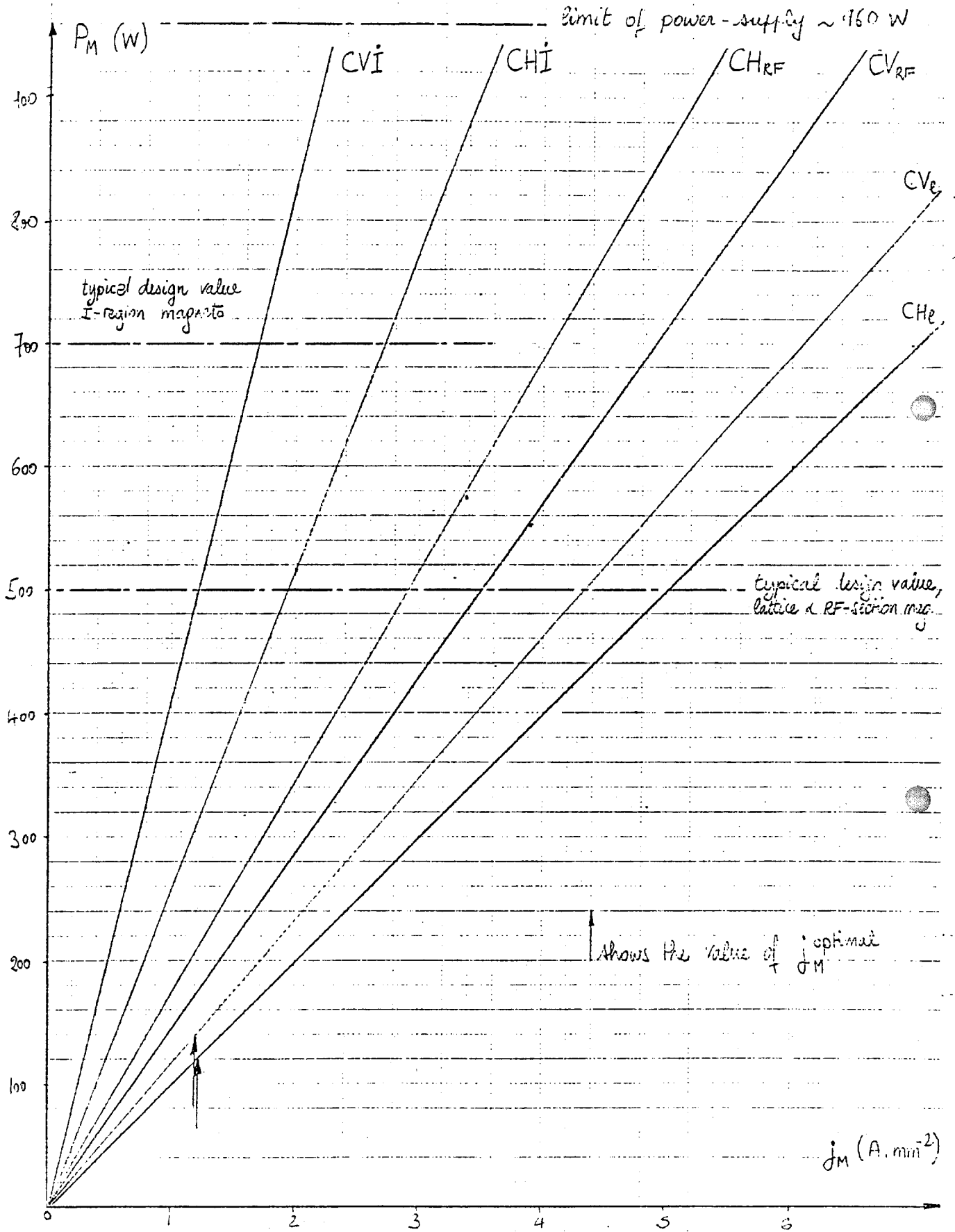
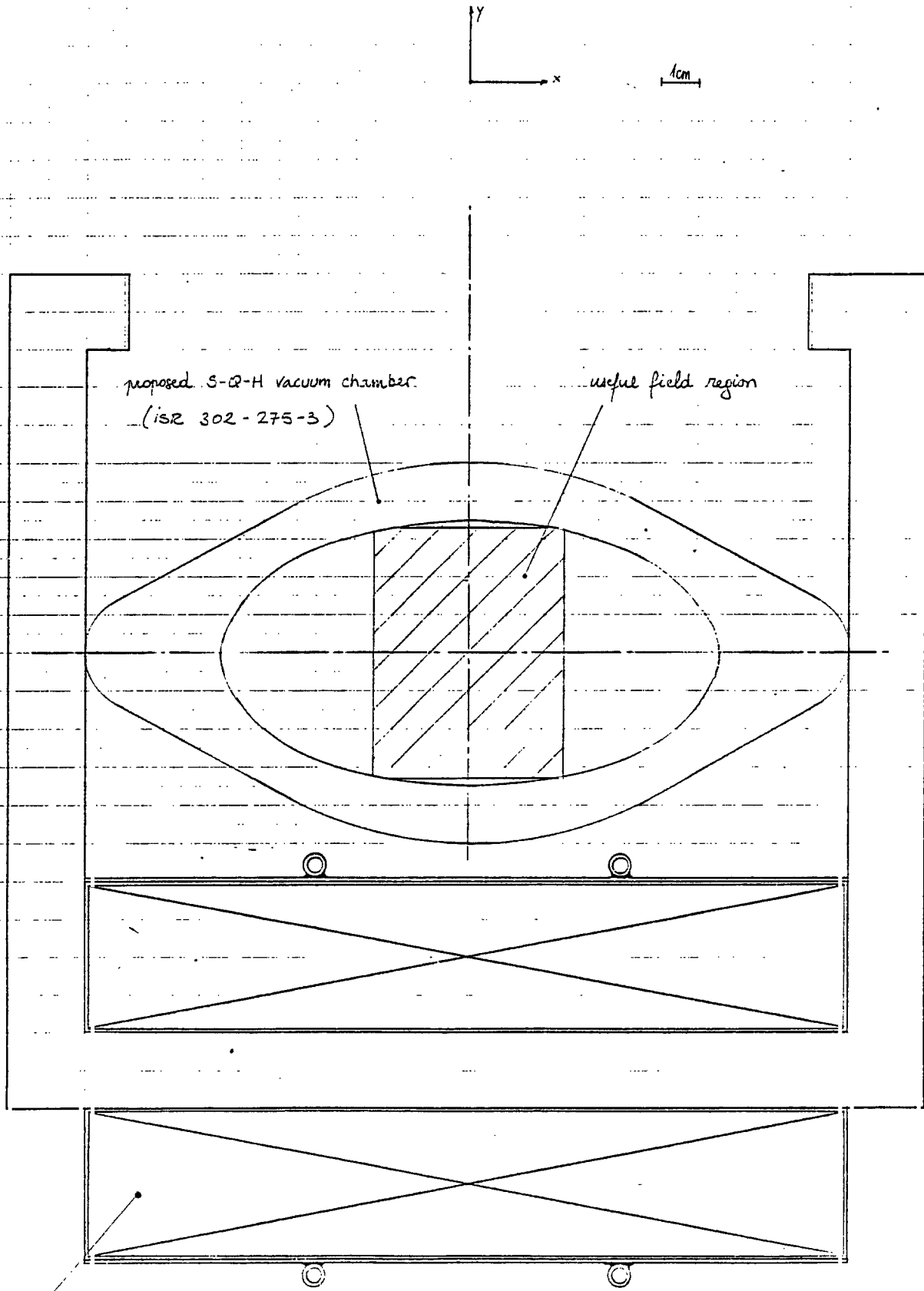


Figure 16 : Magnet power at max. excitation vs. current density in conductor.



- Figure 17: Transverse cross-section of proposed CV lattice magnet -



coil ( 2540 turns,  $\phi$  1.6 mm Cu wire )

- Figure 18 : Calculated field at full excitation, proposed  $CV_{lattice}$  magnet.

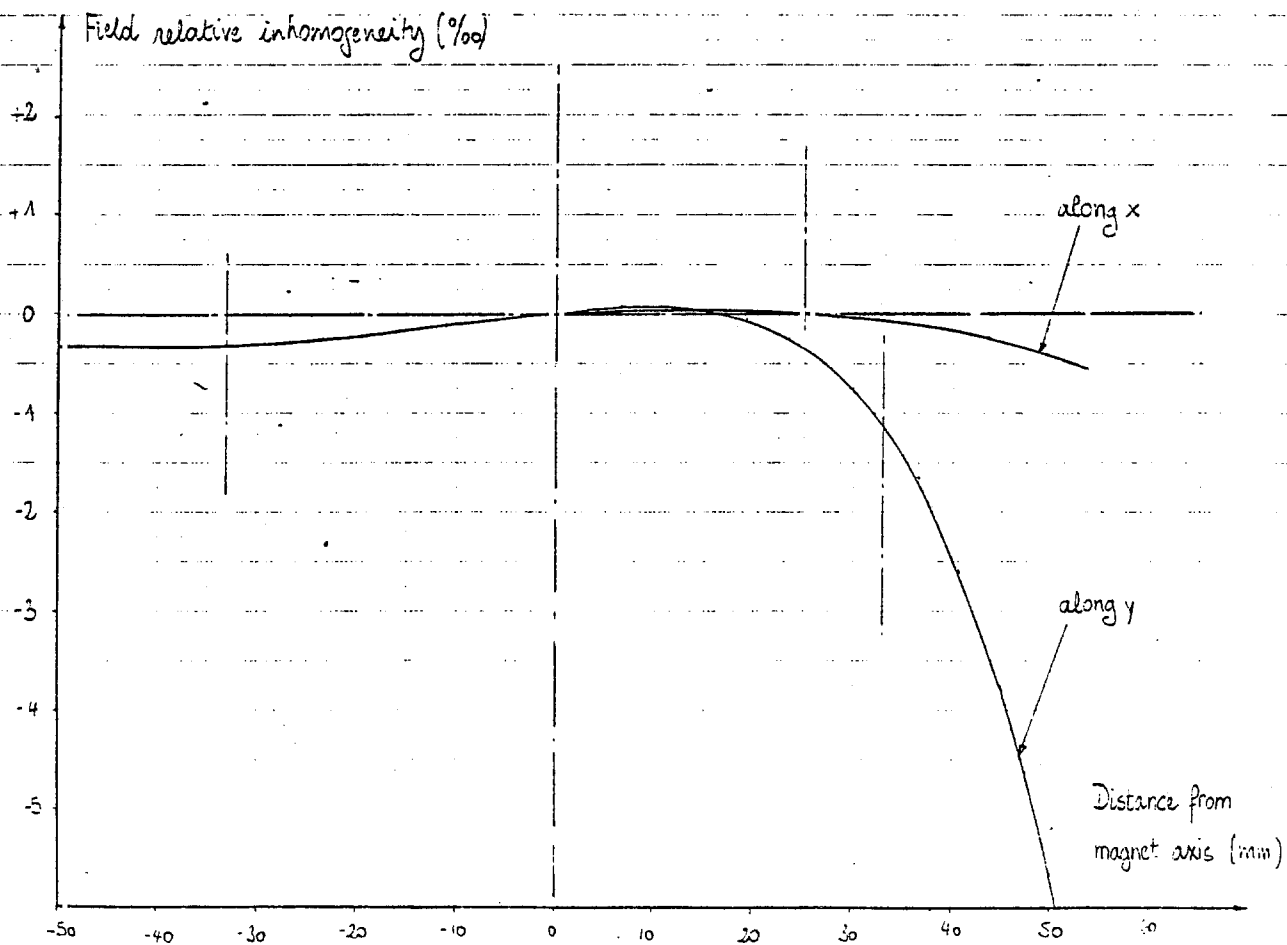
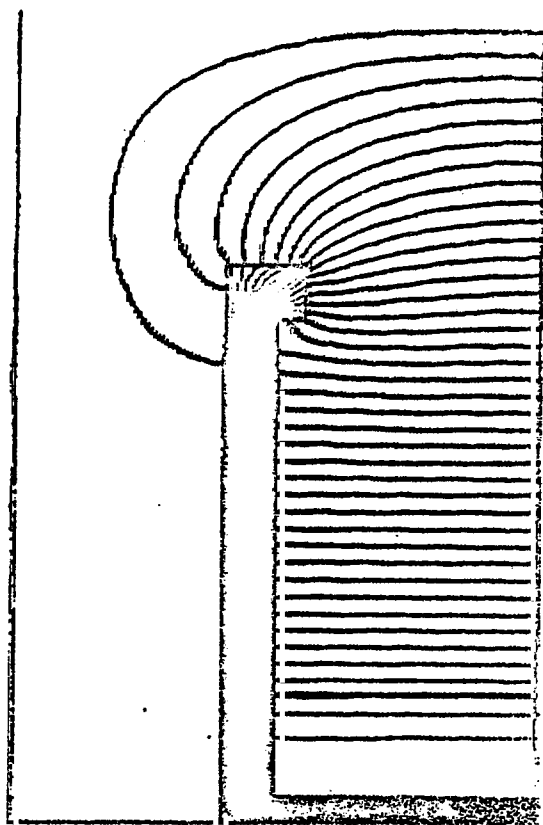
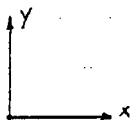
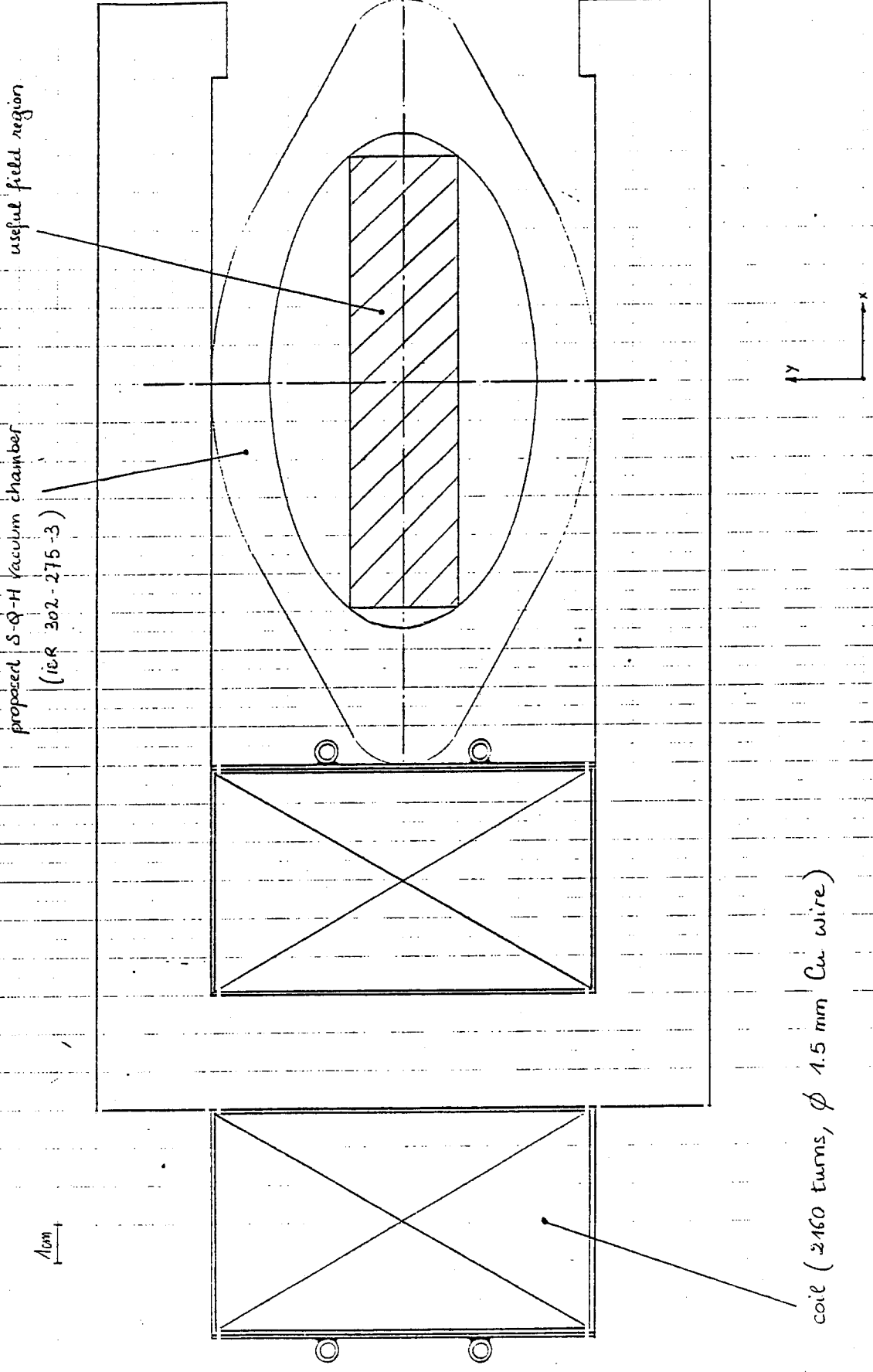


Figure 19: Transverse cross-section of proposed CHEATRICE magnet -



useful field region

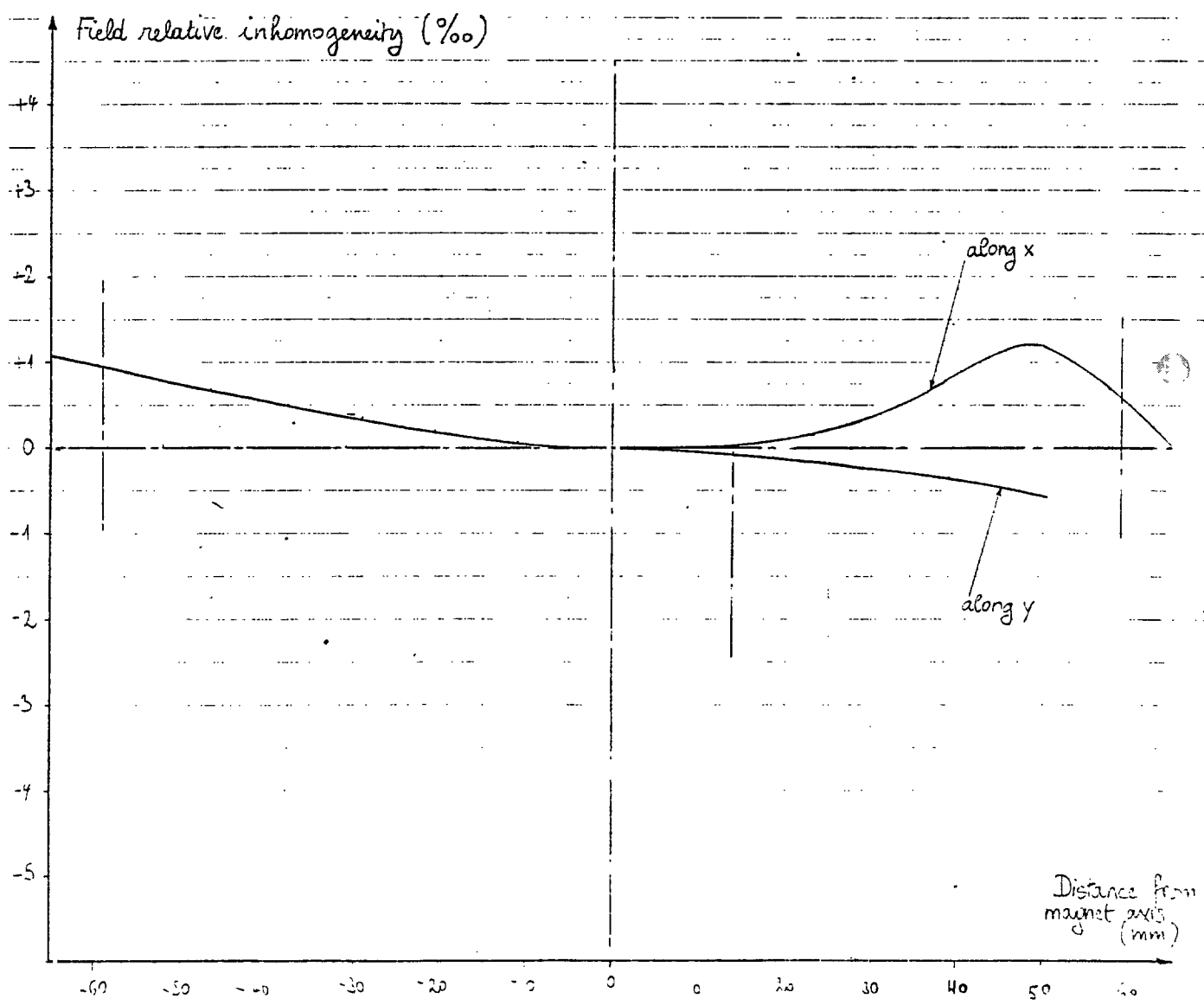
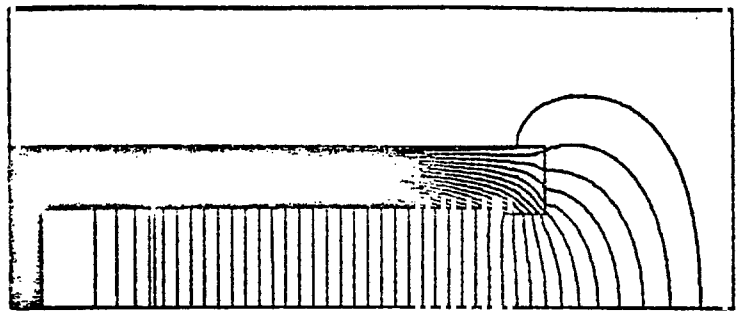
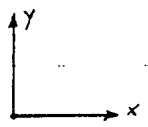
proposed S-Q-H vacuum chamber  
(IBR 302-275-3)

1cm

y  
x

coil (2160 turns,  $\phi$  1.5 mm Cu wire)

Figure 20: Calculated field at full excitation, proposed  $CH_{\text{exitice}}$  magnet -



- Figure 21: Transverse cross-section of proposed  $CV_{RF}$  magnet -

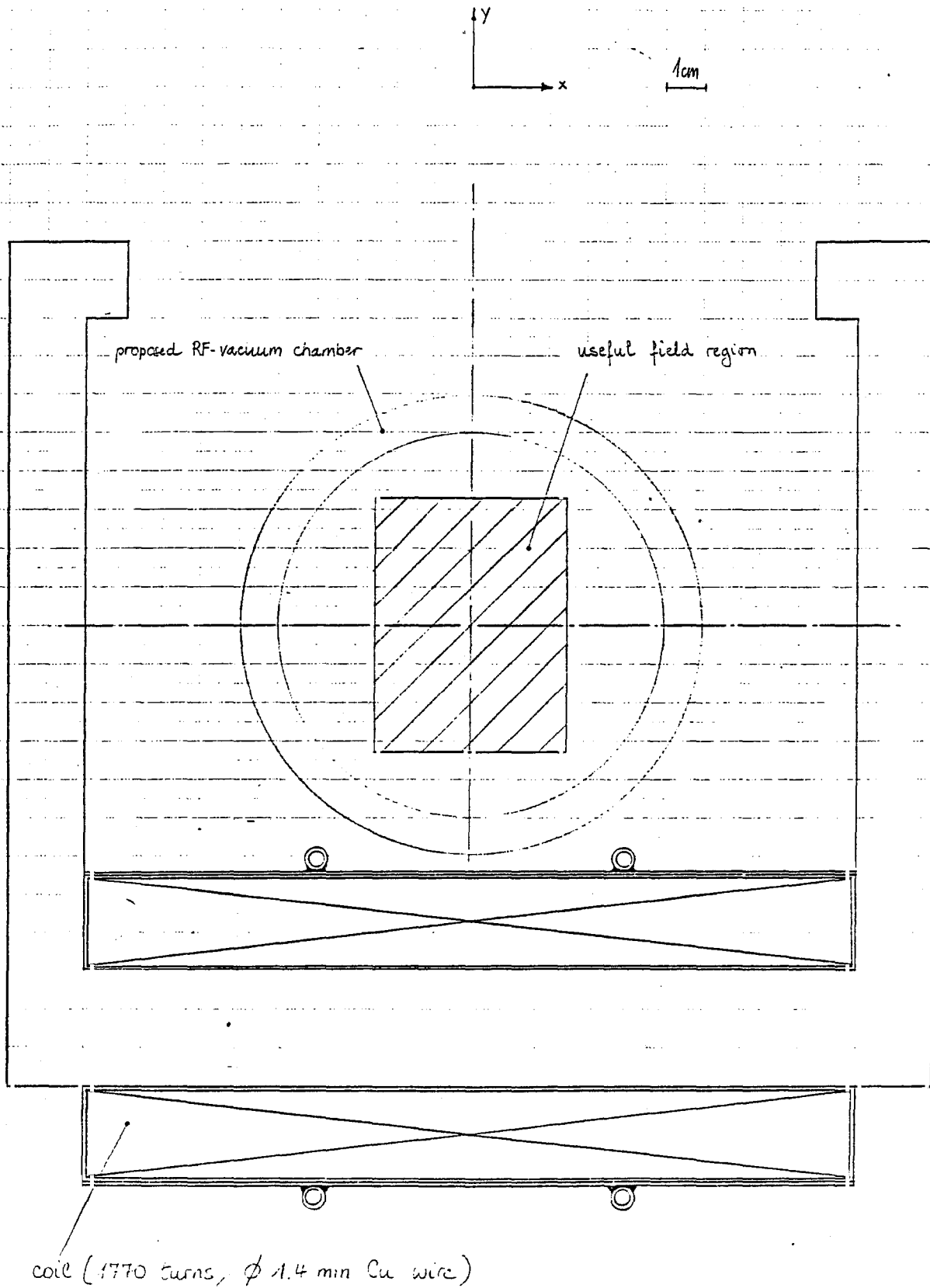


Figure 22: Calculated field at full excitation, proposed CV<sub>RF</sub> magnet.

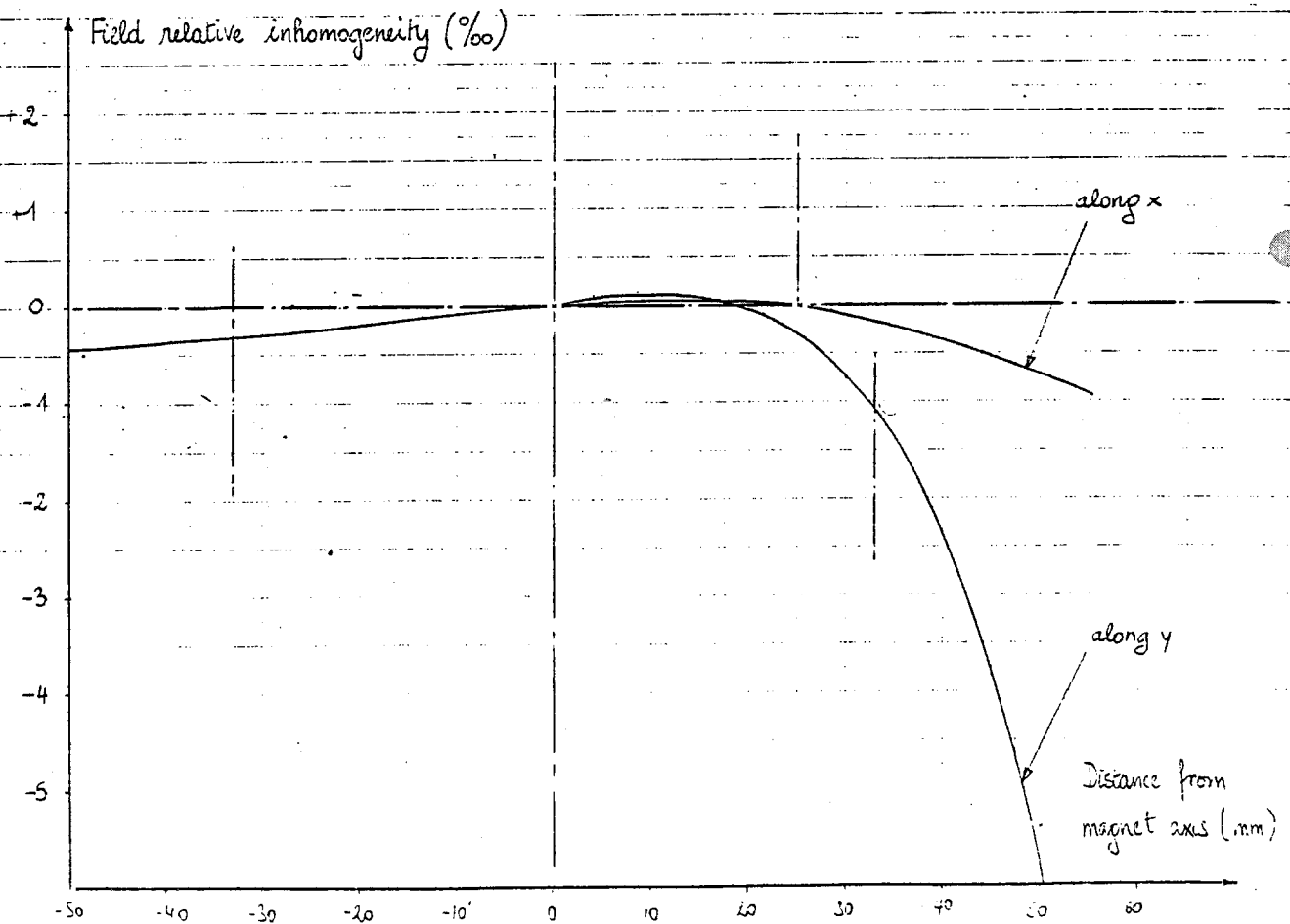
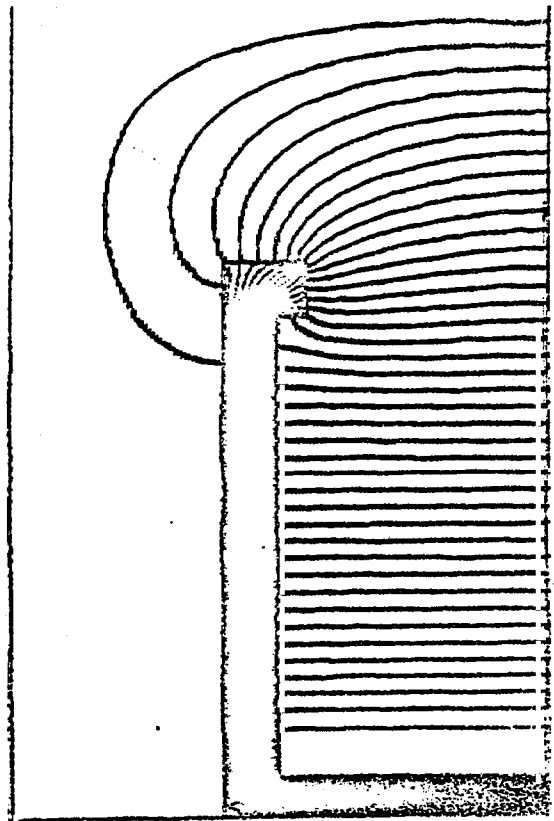
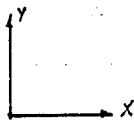
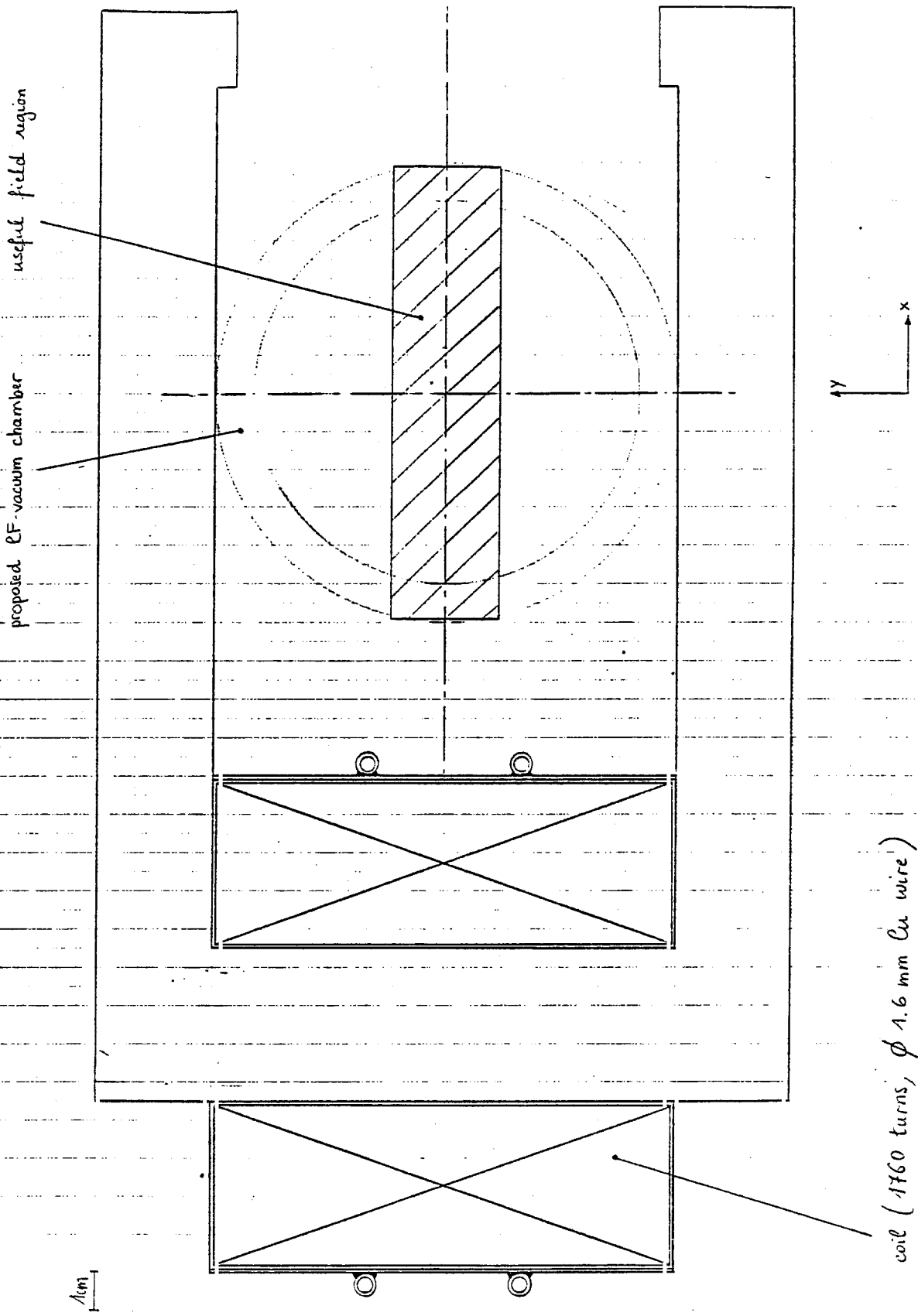
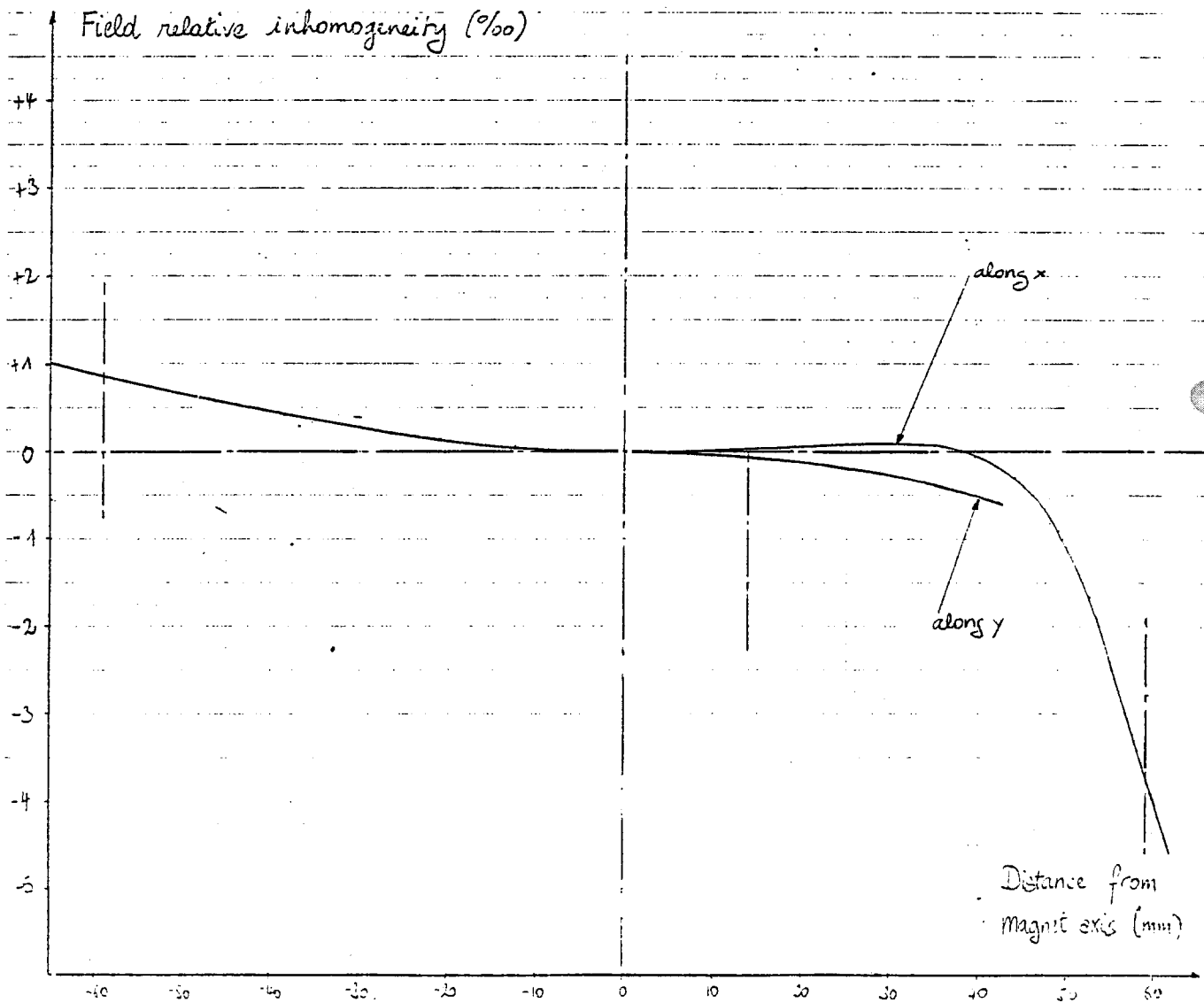
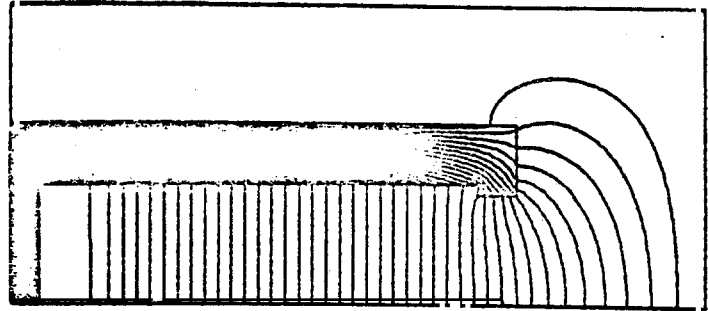
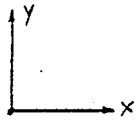


Figure 23: Transverse cross-section of proposed C.H. RF magnet -



coil (1760 turns,  $\phi$  1.6 mm Cu wire)

- Figure 24 : Calculated field at full excitation, proposed  $CH_{RF}$  magnet.



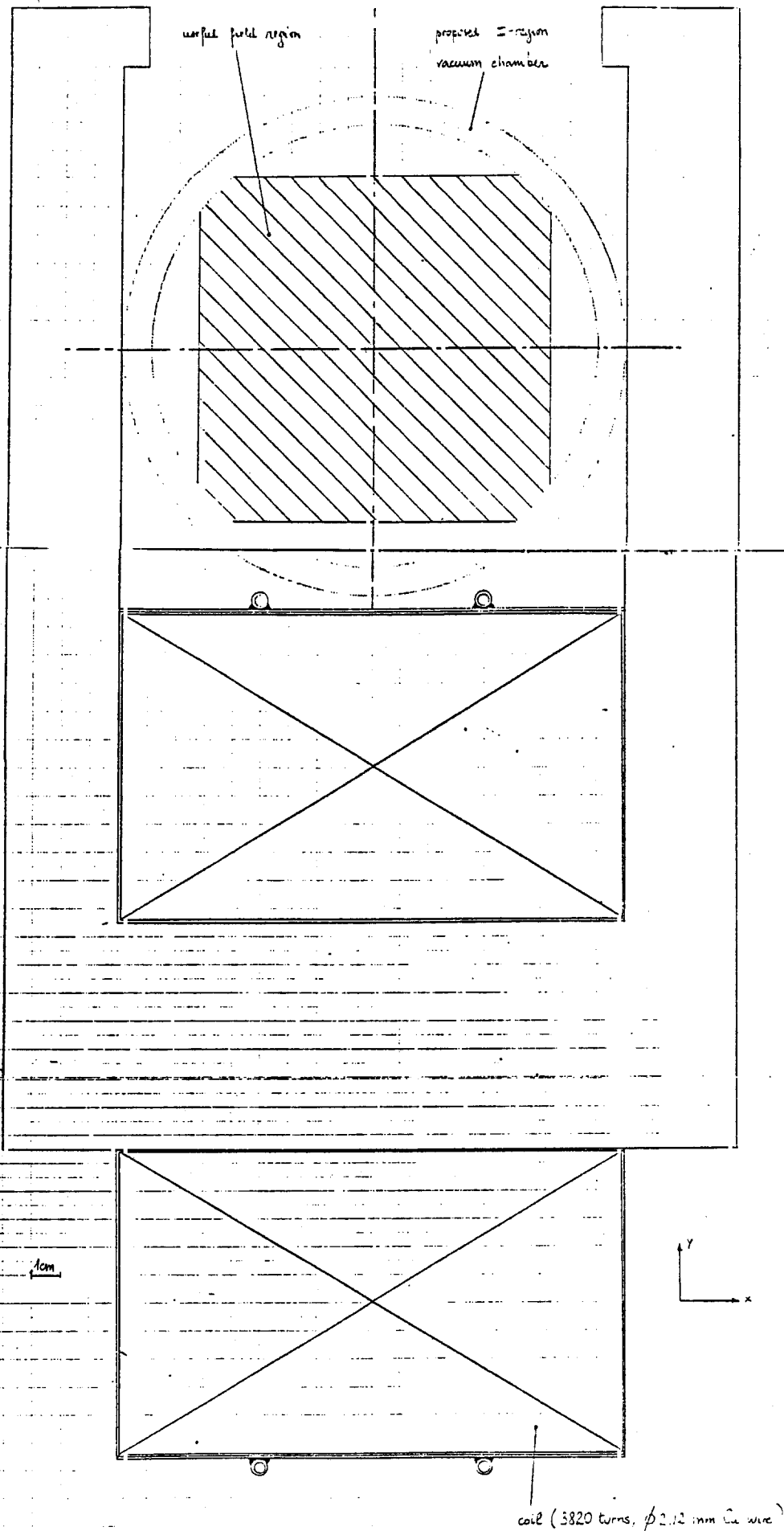


Figure 25: Transverse cross-section of proposed CVT magnet.

- Figure 26 : Calculated field at full excitation, proposed CVI magnet.

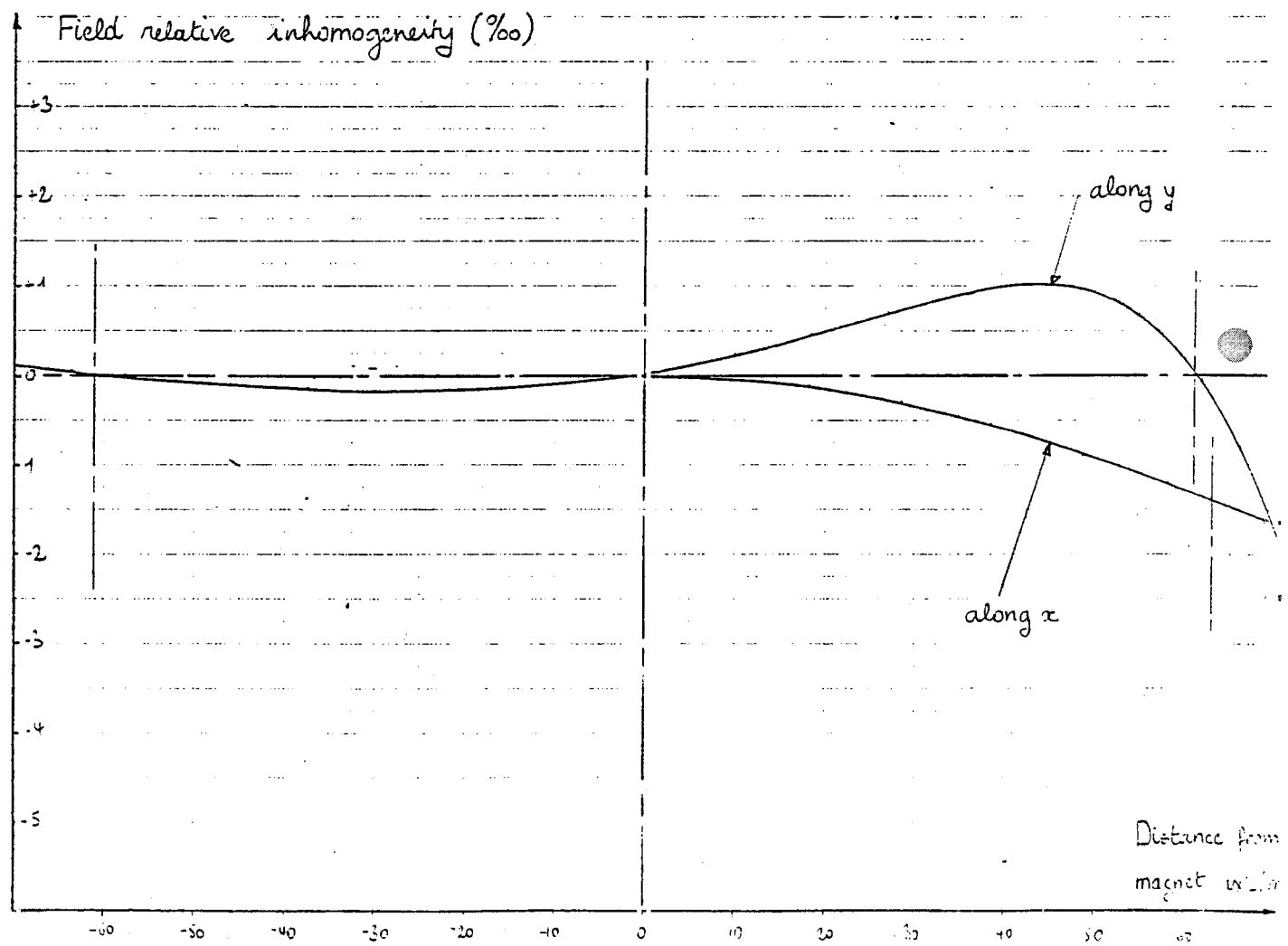
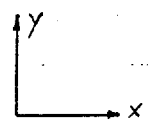
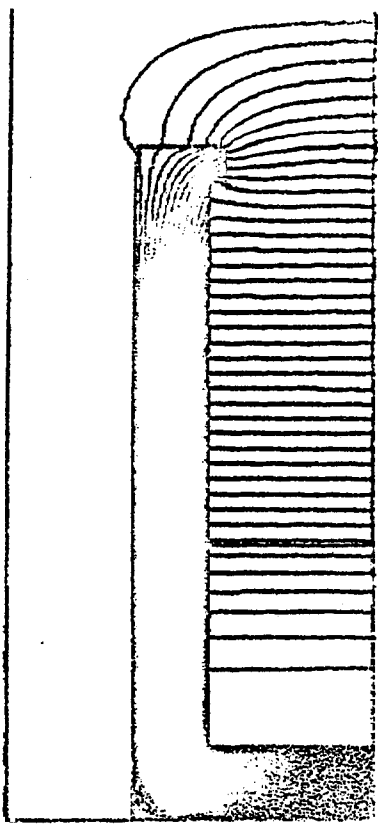
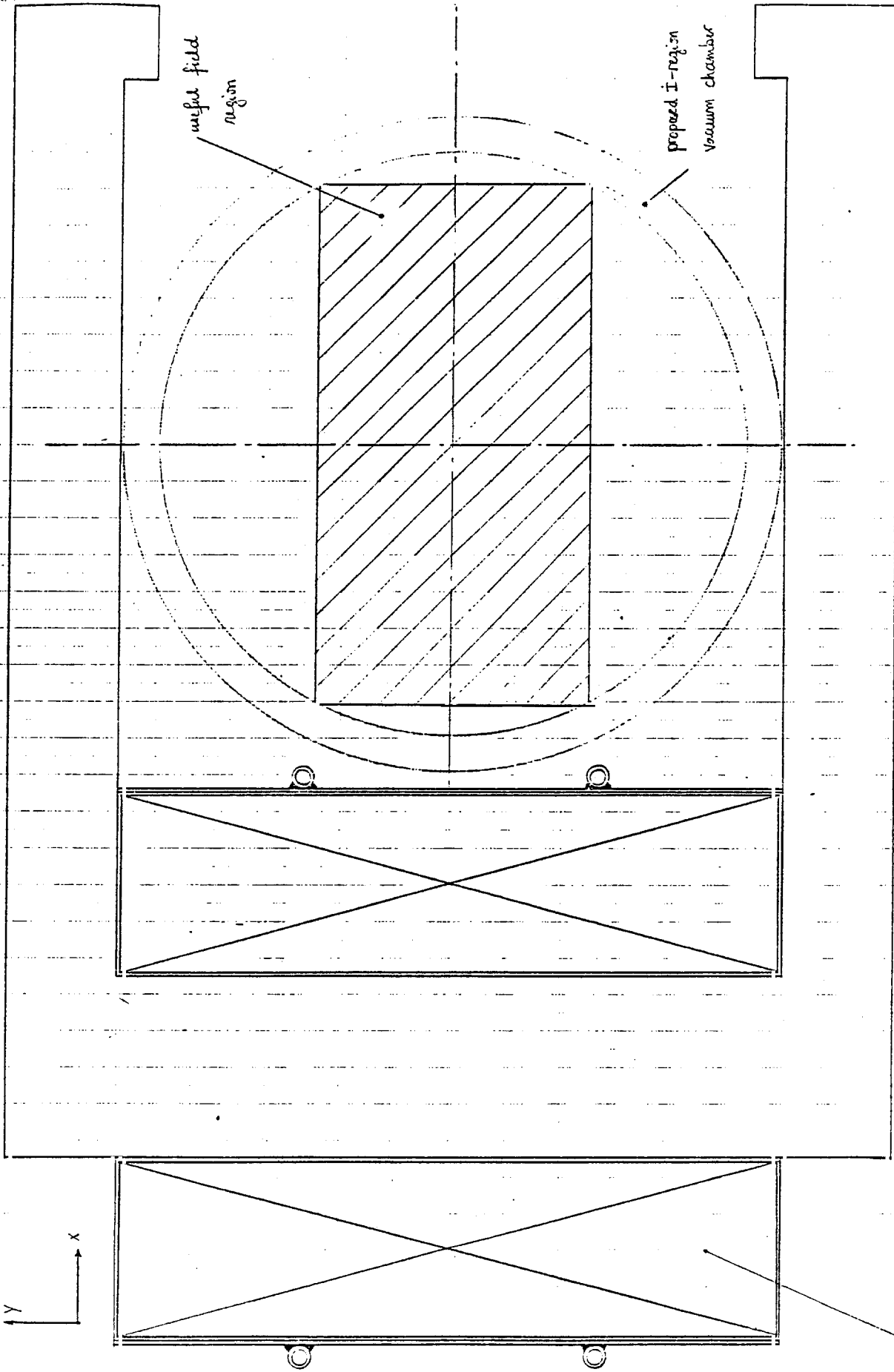
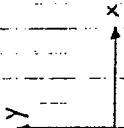


Figure 27: Transverse cross-section of proposed CHI magnet.



coil (2390 turns,  $\phi$  1.8 mm Cu. wire)

Figure 28: Calculated field at full excitation, proposed CHI magnet.



Field relative inhomogeneity (%/oo)

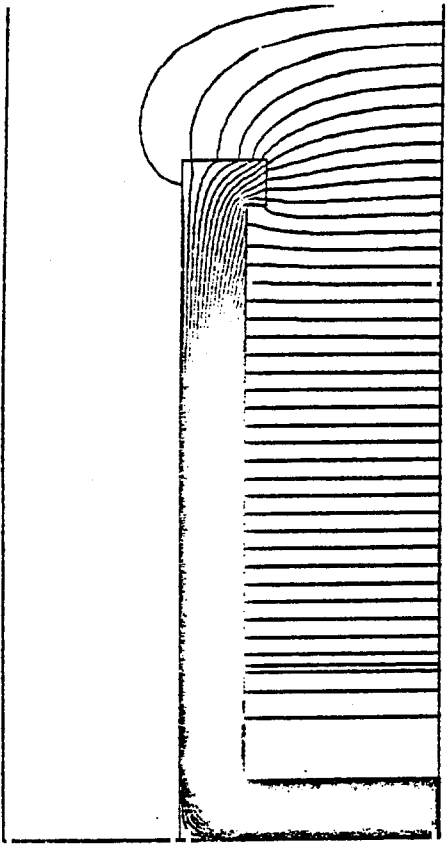
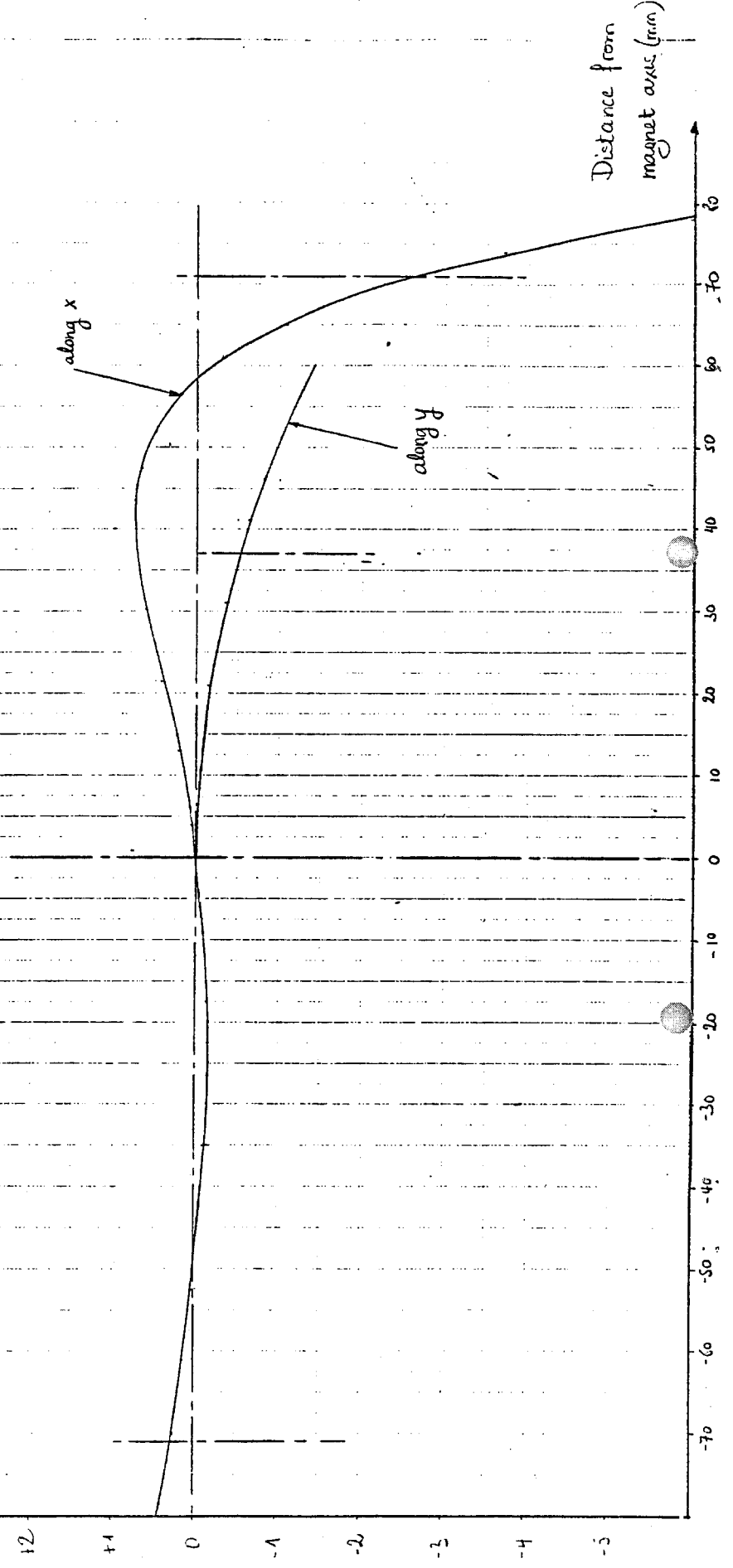


Figure 29: Magnetic properties of non-oriented silicon steels -

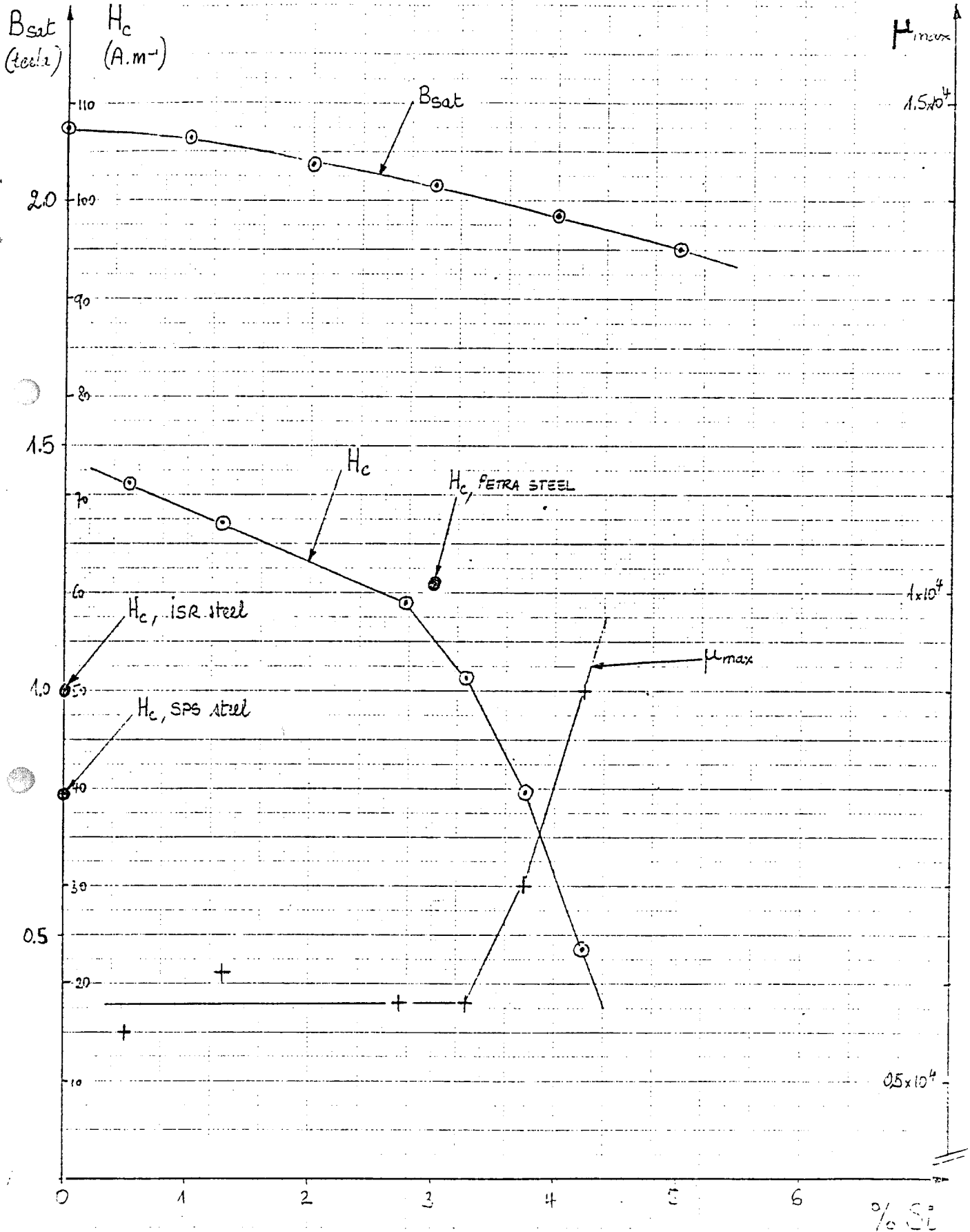


Figure 30: Linear price of biconductor copper cables

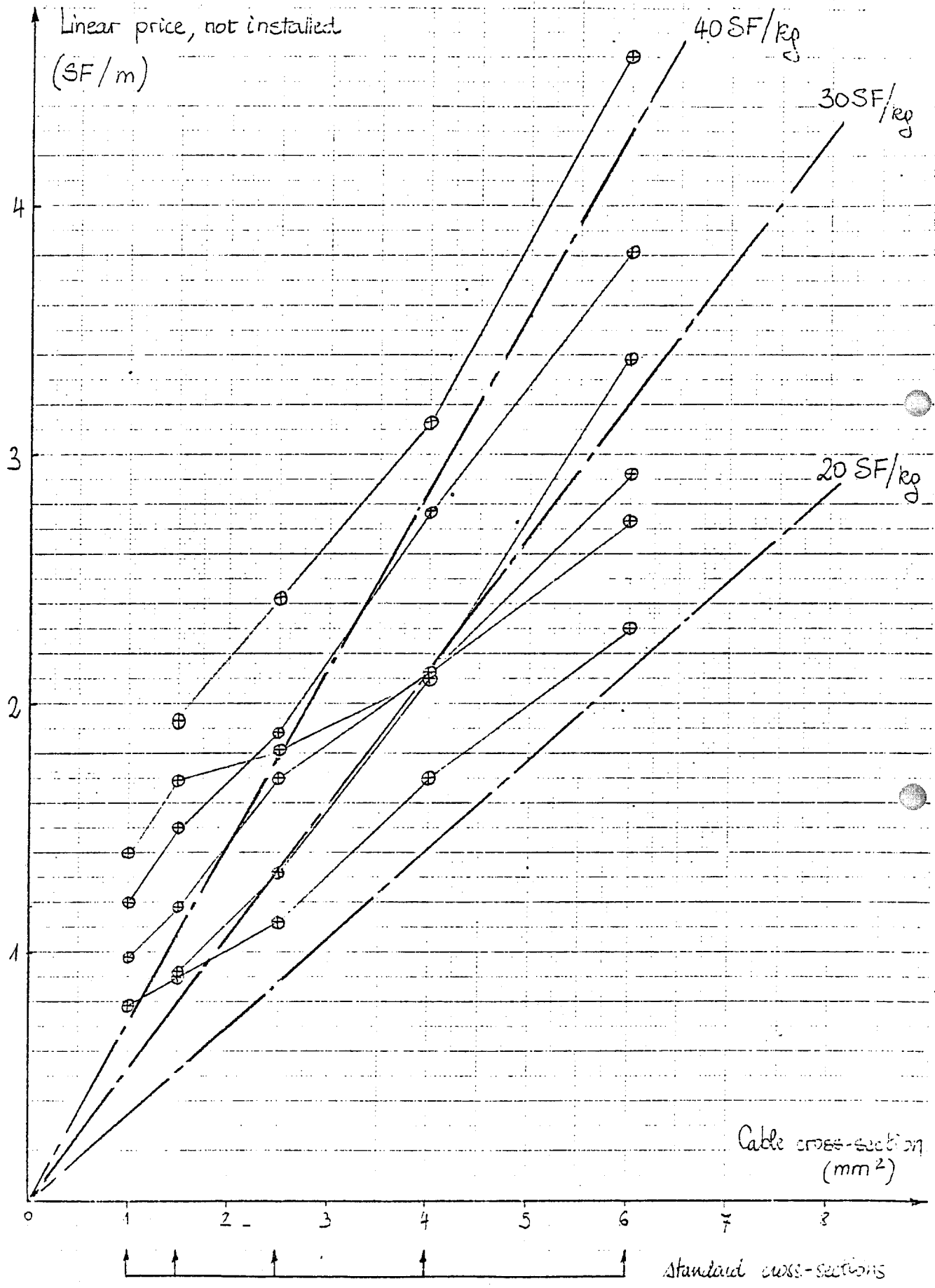
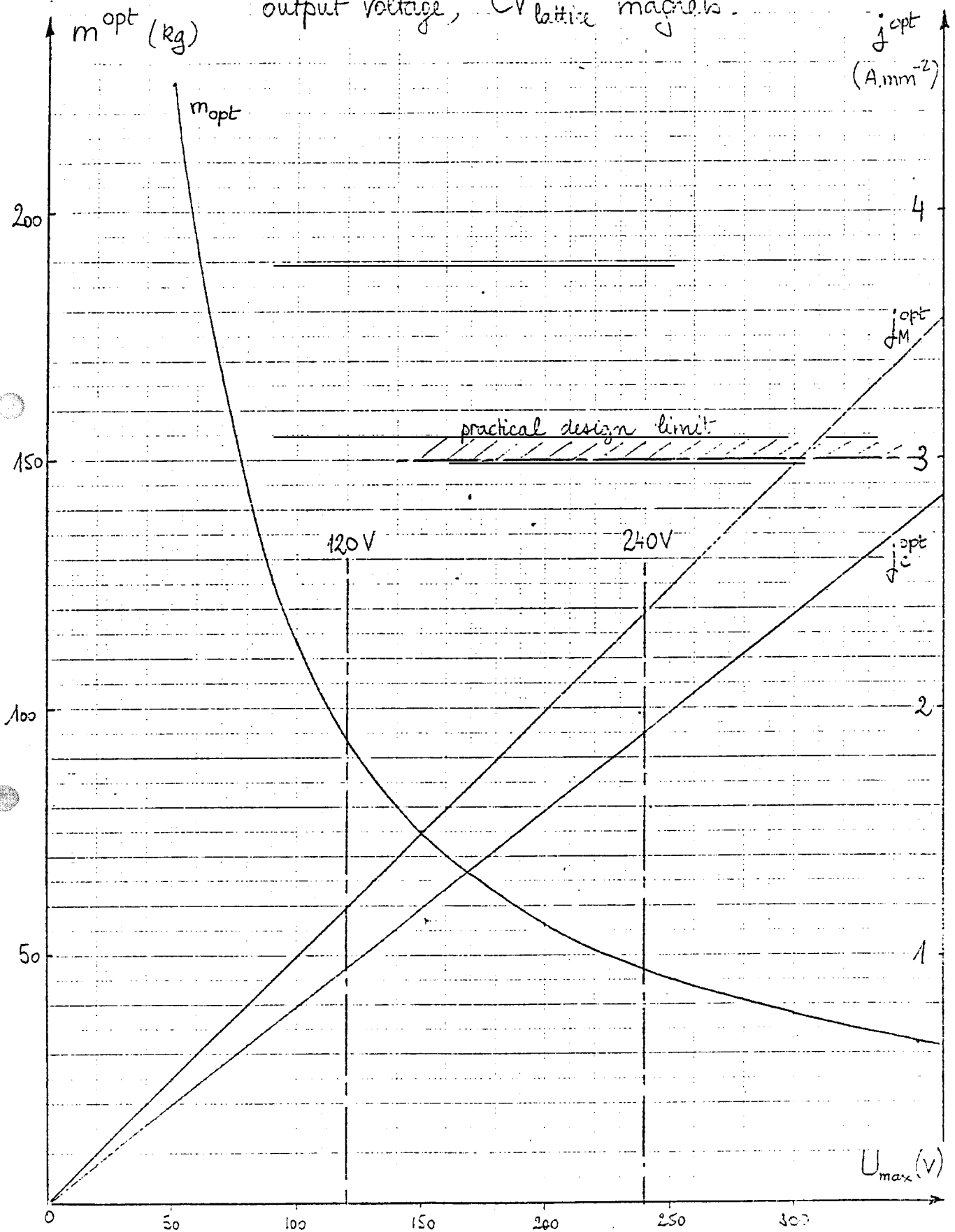


Figure 31: Economic incidence of power-supply maximum output voltage, CV lattice magnets.



- Figure 32: Economic incidence of power-supply maximum

output voltage, CH lattice magnets -

